PFC/RR-84-8

DOE/ET/51013-124
UC-20 a,f

A Time-Resolving Electron Temperature Diagnostic for Alcator C

Stephen A. Fairfax

Plasma Fusion Center
Massachusetts Institute of Technology
Cambridge, MA 02139

May 1984

This work was supported by the U.S. Department of Energy Contract No. DE-AC02-78ET51013. Reproduction, translation, publication, use and disposal, in whole or in part by or for the United States government is permitted.

A TIME-RESOLVING ELECTRON TEMPERATURE DIAGNOSTIC for ALCATOR C

by
Stephen A. Fairfax

B.S. Massachusetts Institute of Technology 1978

Submitted to the Departments of
Electrical Engineering and Computer Science
and
Physics
in Partial Fulfillment of the
Requirements of the Degrees of

MASTER OF SCIENCE IN ELECTRICAL ENGINEERING

and

MASTER OF SCIENCE IN PHYSICS

at the

MASSACHUSETTS INSTITUTE OF TECHNOLOGY

May 1984

Signature of Author: Stephen A. Fairfax
Department of Electrical Engineering

Certified by: Ronald R. Parker
Thesis Supervisor

Certified by: Claude R. Canizares
Thesis Reader

Accepted by: _____
Electrical Engineering Departmental Committee

Accepted by: _____
Physics Departmentmental Committee

ABSTRACT

A diagnostic that provides time-resolved central electron temperatures has been designed, built, and tested on the ALCATOR C tokamak. The diagnostic uses an array of fixed-wavelength x-ray crystal monochromators to sample the x-ray continuum and determine the absolute electron temperature. The resolution and central energy of each channel were chosen to exclude any contributions from impurity line radiation. This document describes the need for such a diagnostic, the design methodology, and the results with typical ALCATOR C plasmas. Sawtooth (m=1) temperature oscillations were observed after pellet fueling of the plasma. This is the first time that such oscillations have been observed with an X-ray temperature diagnostic.

Table of Contents

Introduction.....4

X-ray Emission from a Hot Plasma.....8

Bremsstrahlung.....8

Radiative Recombination.....14

Resonant Transitions.....18

Electron Temperature Measurement Techniques.....20

Thomson Scattering.....20

Electron Cyclotron Emission.....22

X-ray Continuum Techniques.....23

Requirements for a New Electron Temperature Diagnostic.26

Description of the Instrument.....38

Relative Advantages of Analog and Counting Modes....42

Results.....46

Counting Mode Operation.....47

Analog Mode Operation.....60

Future Work.....66

Acknowledgements.....68

References.....69

INTRODUCTION

The inevitable depletion of fossil fuel supplies has led this nation and others to search for new, inexhaustable sources of energy. Controlled thermonuclear fusion is an attractive possibility for several reasons. The fuels required are naturally abundant and cheap, the environmental impact seems manageable, and waste disposal problems are small compared to those of fission or fossil-fuel technologies. Controlled fusion has proven to be extremely difficult to implement; almost 30 years of research have been required to build a device that may produce as much energy as is required to heat it.

There are many approaches to fusion, but one has emerged as a clear leader in the race for energy production. The tokamak was invented by the Russian physicists Tamm and Sakharov in 1951 [1]. The tokamak uses a strong toroidal magnetic field generated by external magnets combined with a poloidal magnetic field generated by current in the plasma for confinement. The toroidal current heats the plasma through ohmic loss to temperatures in the range 1-3 KeV. (1 eV = 11,600 degrees K) Energy production requires temperatures in the range of 6 - 20 KeV, so auxiliary heating methods are required.

The ALCATOR C tokamak is currently in operation at the Plasma Fusion Center at MIT. The ALCATOR program utilizes the high-field magnet technology developed at the Francis

Bitter National Magnet Laboratory to construct tokamaks with very high toroidal magnetic fields. ALCATOR C operates with toroidal fields up to 14 Tesla, approximately 3-5 times that of most other tokamaks. The very high magnetic field supports the confinement of high density plasmas with current densities in excess of 1 KA/cm^2. High magnetic fields also allow for the construction of compact devices. ALCATOR C has a major radius of only 64 cm and a minor radius of 16 cm, compared to machines of comparable power and performance with radii of meters and magnetic fields of 2-3 Tesla.

ALCATOR C is a high-performance tokamak; It does 0-14 Tesla in 1.5 seconds, 0-800 KA in 500 msec, and 800-0 KA in 1 msec. It is turbo-pumped, fuel-injected, and cryogenically cooled, with a 220,000 hp power supply. ALCATOR C holds many world records in the areas of plasma particle density, current density, power density and impurity levels. It is presently the only machine to have achieved a value of plasma density times energy confinement time sufficient for energy break-even.

There are some drawbacks with ALCATOR-type tokamaks. The primary difficulty is access to the plasma. The "Bitter plate" construction technique used encloses the entire plasma chamber with up to 50 cm of copper and stainless steel. Physical and optical access is granted only by insertion of stainless-steel wedges with machined holes in the magnet assembly. Insertion to these 'flanges' introduces undesirable ripple in the toroidal magnetic field and reduces the

space available for current-carrying magnet plates. A compromise is required; ALCATOR C has 6 flanges spaced 60 degrees apart around the torus. Each flange has access ports on the top, bottom, and outside edge, for a total of 18. A fully instrumented tokamak requires up to 50 diagnostics and experiments. Most instruments are designed to share port space, and the diagnostic array is changed frequently.

Table 1 includes a summary of ALCATOR C parameters, and figure 1 shows a schematic of the machine.

ALCATOR C PARAMETERS

Major Radius	$R = 64$ cm
Minor Radius	$a = 16$ cm
Toroidal Magnetic Field	$B_T \leq 14$ Tesla
Plasma Current	$I_p \leq 1$ MA
Plasma Density	$n \leq 2 \times 10^{15}$ cm^{-3}
Electron Temperature	$T_e \leq 3$ KeV
Ion Temperature	$T_i \leq 2$ KeV
Energy Confinement Time	$\tau \leq 50$ msec
Lawson Product	$n\tau \leq 1 \times 10^{14}$ sec/cm^3
RF Heating Power	$P_{LHH} \leq 4$ MW @4.6 GHz
	$P_{ICRF} \leq 2$ MW @200 MHz
Peak Power Requirement	$P_p < 240$ MW$_e$

Table 1

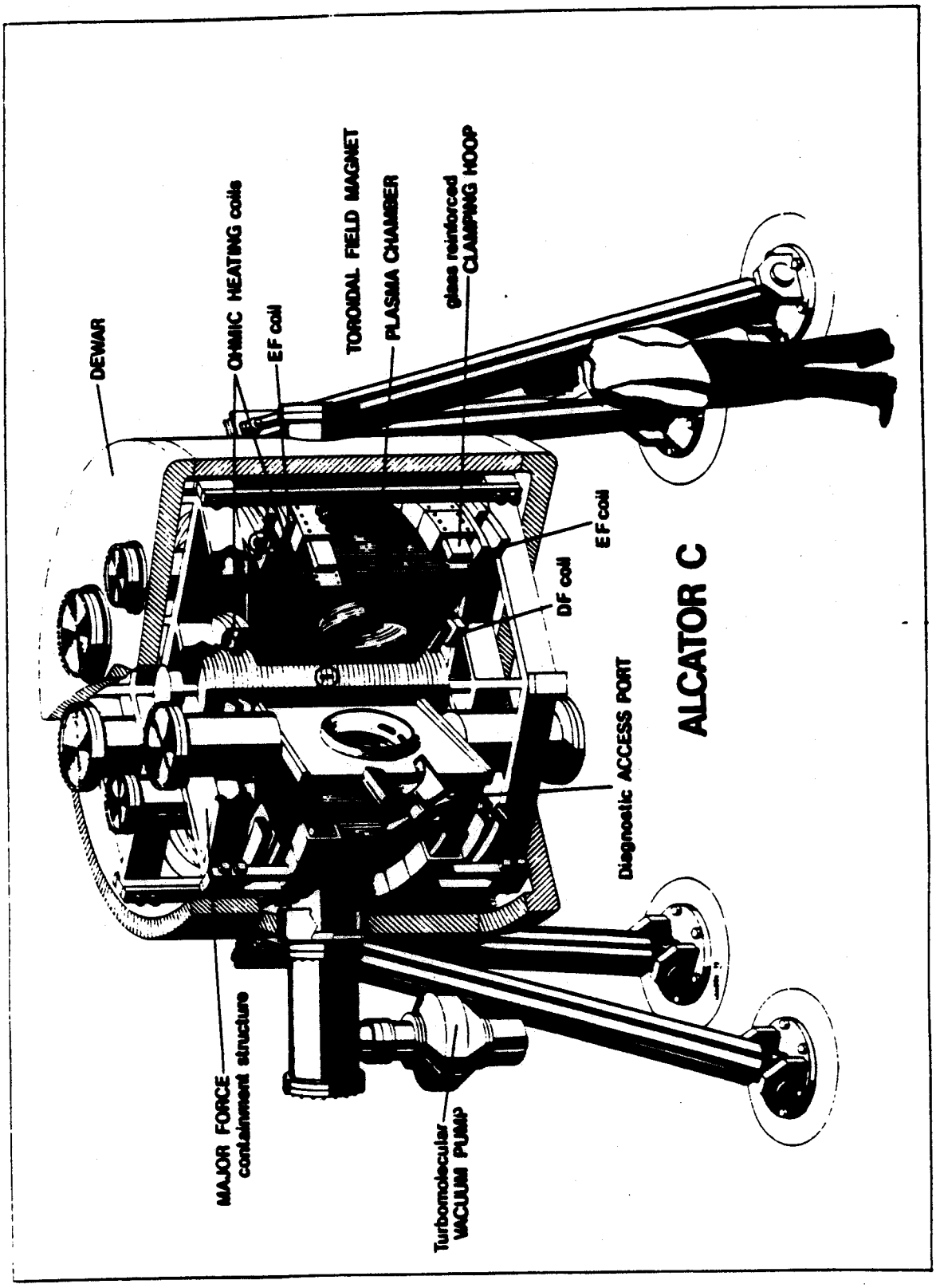

Figure 1
Cut-Away Drawing of ALCATOR C

X-ray Emission from a Hot Plasma

A hot plasma emits radiation at a wide range of wavelengths via a multitude of processes. In the x-ray region where $h\nu < kT_e$, three processes are important. They are bremsstrahlung, radiative recombination, and resonant transition.

BREMSSTRAHLUNG

Bremsstrahlung is the result of electon-electron and electron-ion collisions in the plasma. The initial and final states of particles in a bremsstrahlung collision are unbound, and so the photons emitted comprise a continuous spectrum. A complete treatment of the problem requires the initial and final state wave functions for the positive energy states of the radiating particle, and computation of the electric dipole radiation matrix elements. Expressions for the later do not exist in closed form and must be integrated numerically. Sommerfeld and Maue [2] found a closed-form expression for the bremsstrahlung cross section integrated over all angles of the emitted photon. The integrated cross section may be convolved with an isotropic electron velocity distribution function to yield the energy spectrum of x-rays emitted by bremsstrahlung in a plasma with stationary ions. For a Maxwellian electron distribution function of temperature T_e, the convolution gives [3]:

$$I(h\nu) = 2.6\times10^{-14}\, n_e \sum_i Z_i^2 \sqrt{13.6eV/T_e}\; \bar{g}\; \exp[-h\nu/kT_e] \quad \frac{\text{watts}}{\text{unit\_energy-cm}^3}$$

where n_e is the electron density, n_i the ion density, Z_i the charge of the stationary ions, and $\bar{g}$ the velocity-averaged gaunt factor [4].

The plasma is optically thin at x-ray wavelengths, and any measurement of the x-ray spectrum at a particular plasma radius results in a line integral of all x-rays emitted along that chord in the direction of the detector. ALCATOR C plasmas exhibit gaussian temperature profiles whose 1/e width (a_T) is determined by the ratio of the toroidal magnetic field (B_T) and poloidal current (I_p). The relation between a_T, B_T, and I_p has been determined to be [5]:

EQ1 $$a_T = 4.2(I_p/B_T)^{1/2} \text{ cm}$$

ALCATOR is usually run with the ratio of I_p and B_T such that the profile 1/e width is 10 cm. The density profile depends upon the particular plasma parameters, but is usually well modeled by a parabola to the 1/2 power. These profiles can be integrated with the bremsstrahlung cross-section given above to yeild the expected line-integrated spectrum. The results of such a line integral are shown in Figure [2]. At photon energies $h\nu>2T_e$, the spectrum is well modeled by a simple exponential, $I(h\nu) = \exp[-h\nu/kT_o]$. T_o is always lower than the central plasma temperature (T_{eo}) because the low energy portion of the spectrum receives substantial

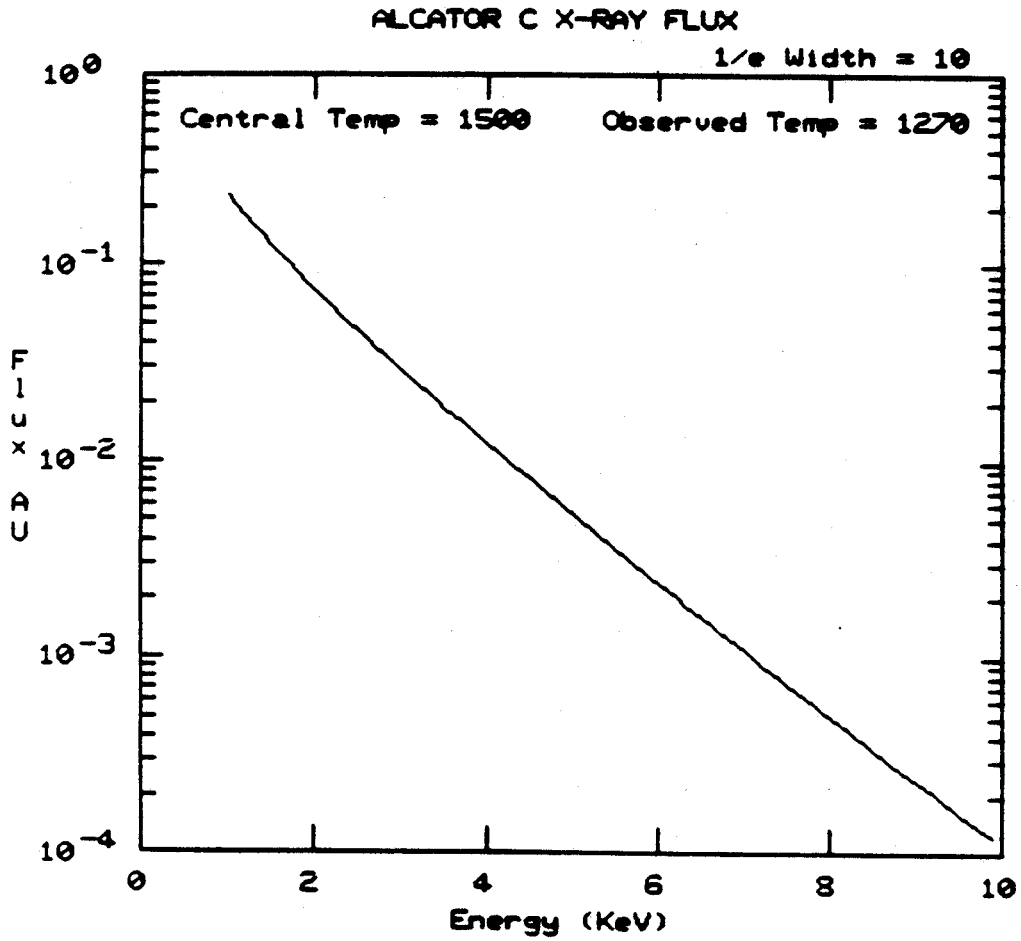

Figure 2
Simulated Bremsstrahlung Flux from ALCATOR C Plasma

contributions from the outer, cooler, regions of the plasma. These outer regions contribute very little to the high-energy portion of the spectrum because the photon energy is so much greater than the local temperature. The quantity of interest is the central electron temperature, so it is necessary to calculate the ratio of the observed temperature to the central temperature over the possible range of temperature and density profiles. This correction factor will be a function of central plasma temperature, temperature profile width, density profile, and region of the spectrum where the exponential is fitted. Fitting at higher energies gives a T_o that is closer to T_{eo} becase the contribution of the outer plasma regions is reduced. The results of a numerical integration are shown in figure [3] for density profiles modeled as $n(r)=[1-(r/16)^2]^s$, where s is between .5 and 2. Peaked profiles weight the measurement toward the central portion of the plasma, reducing the correction factor. S is usually equal to .5 during normal ALCATOR discharges. The major exception occurs after pellet fueling of the discharge, when the profile may become more peaked. The density profile very rarely exhibits peaking greater than s = 2 [6].

The variation of the profile correction factor with plasma temperature can be very well approximated with a quadratic in T_o. The approximation for parabola$^{1/2}$ density profiles and gaussian temperature profiles of 1/e width equal to 10 cm is shown in figure [4]. This provides a convenient method of correcting the observed plasma temperature for

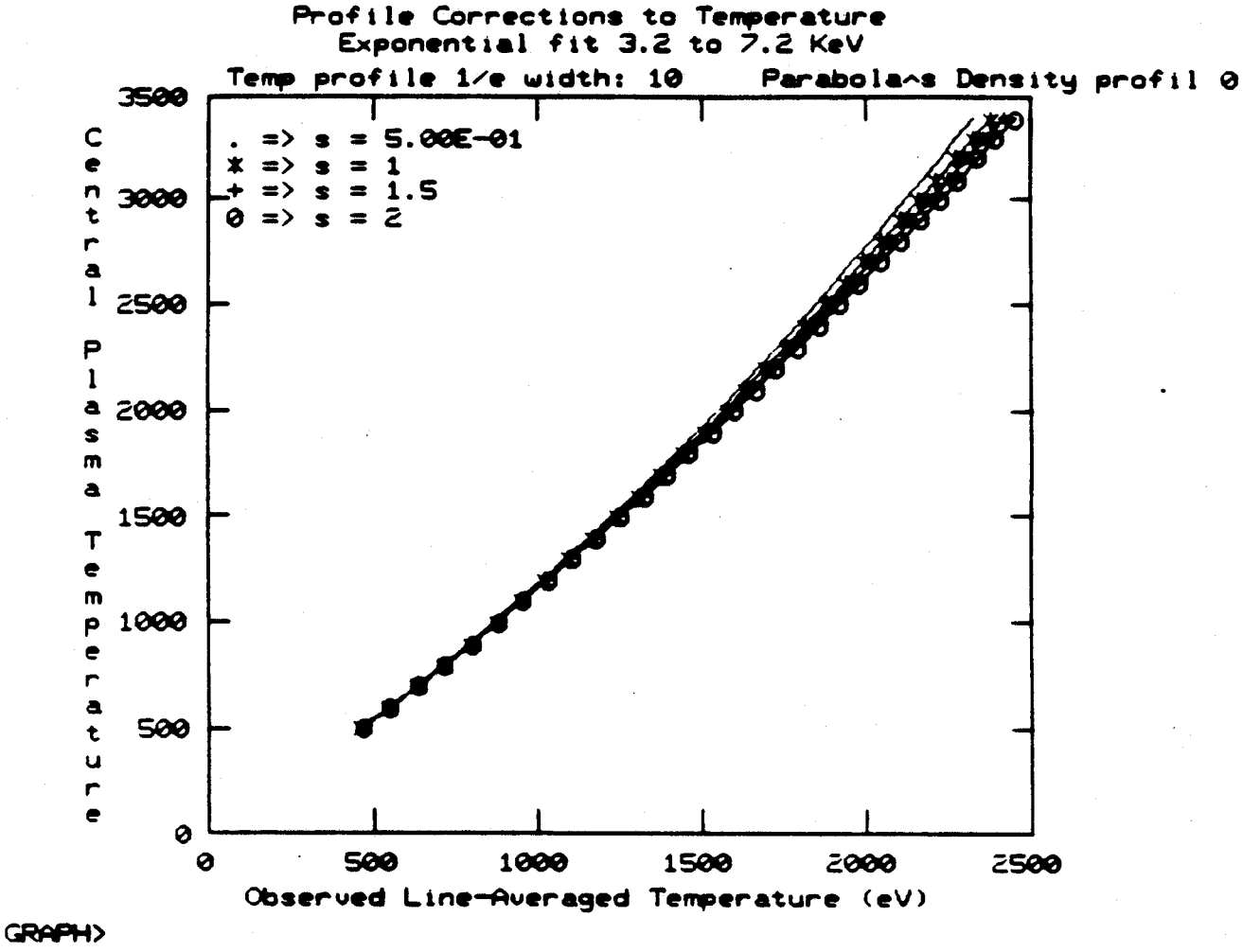

Figure 3
Profile Correction:
Central Temperature vs Observed Temperature
for 4 Density Profiles

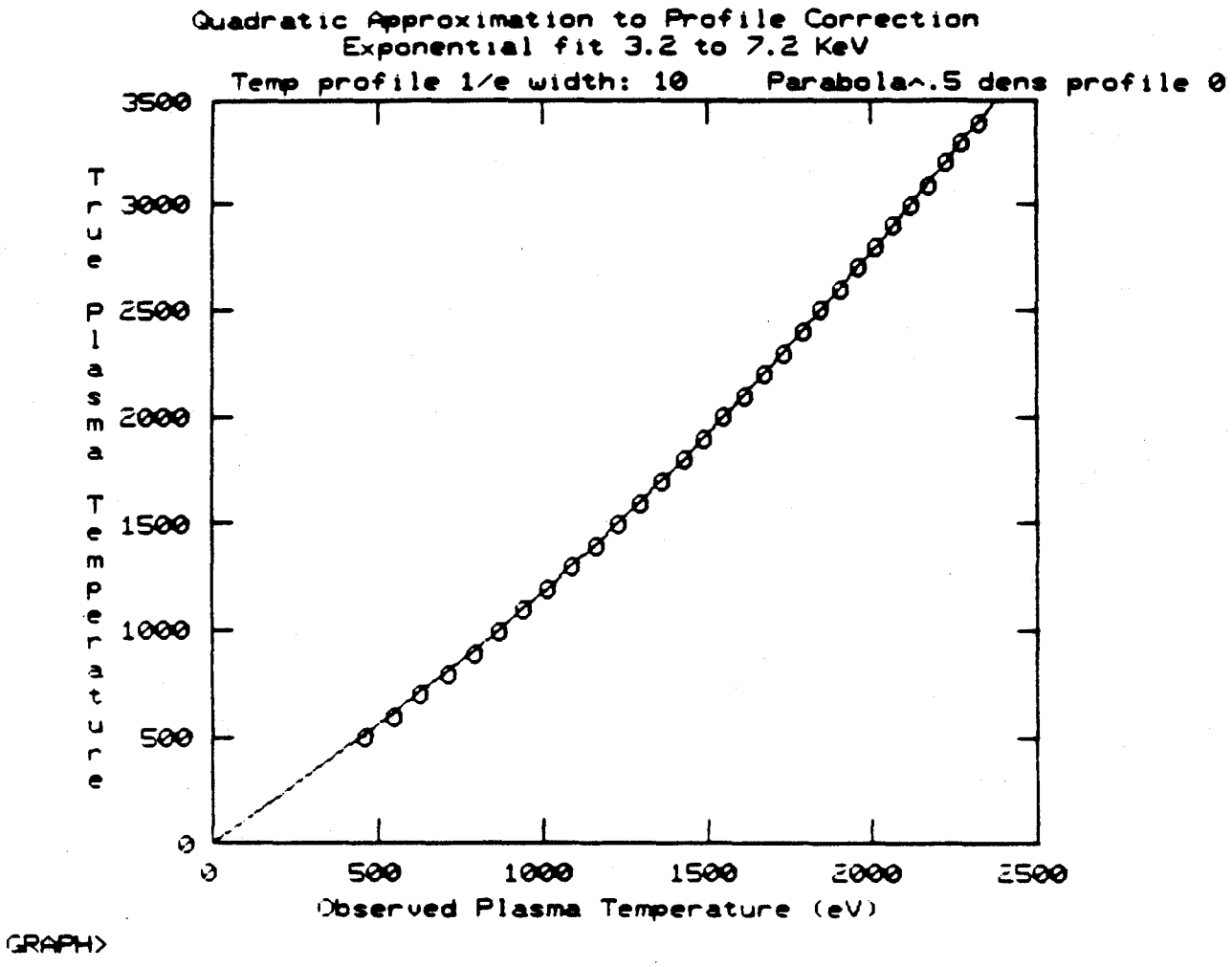

Figure 4
Quadratic Approximation to Profile Correction

profile effects.

It would be possible to include the effects of temperature profile width in the polynomial approximation by making the coeffcients functions of I_p/B_T. The range of I_p/B_T normally encoutered in ALCATOR C discharges is limited except during the plasma current ramp-up, when the x-ray flux is low. The difference between a correction that includes width and that given by the quadratic approximation is typically less than 1%. A plot of correction factor vs. profile width is shown in figure [5]. Because the effect is so small, this additional correction was ignored.

RADIATIVE RECOMBINATION

In the radiative recombination process electrons undergo transitions from free states in a Coulomb field to bound states. The spectrum of emitted photons is continous but has jumps at energies corresponding to the ionization potentials of the final bound levels. The determination of the cross section for this process is similar to that for bremsstrahlung, but the final state wave functions are bound. These wave functions are not well known for high-Z, partially ionized atoms. Detailed treatments were done by Menzel and Pekeris [7], Karzas and Latter [4], Brussaard and van de Hulst [8], (who considered the case of the emitted spectrum from a Maxwellian electron distribution), and by Von Goeller [9]. The essential result is that g in equation [1] is

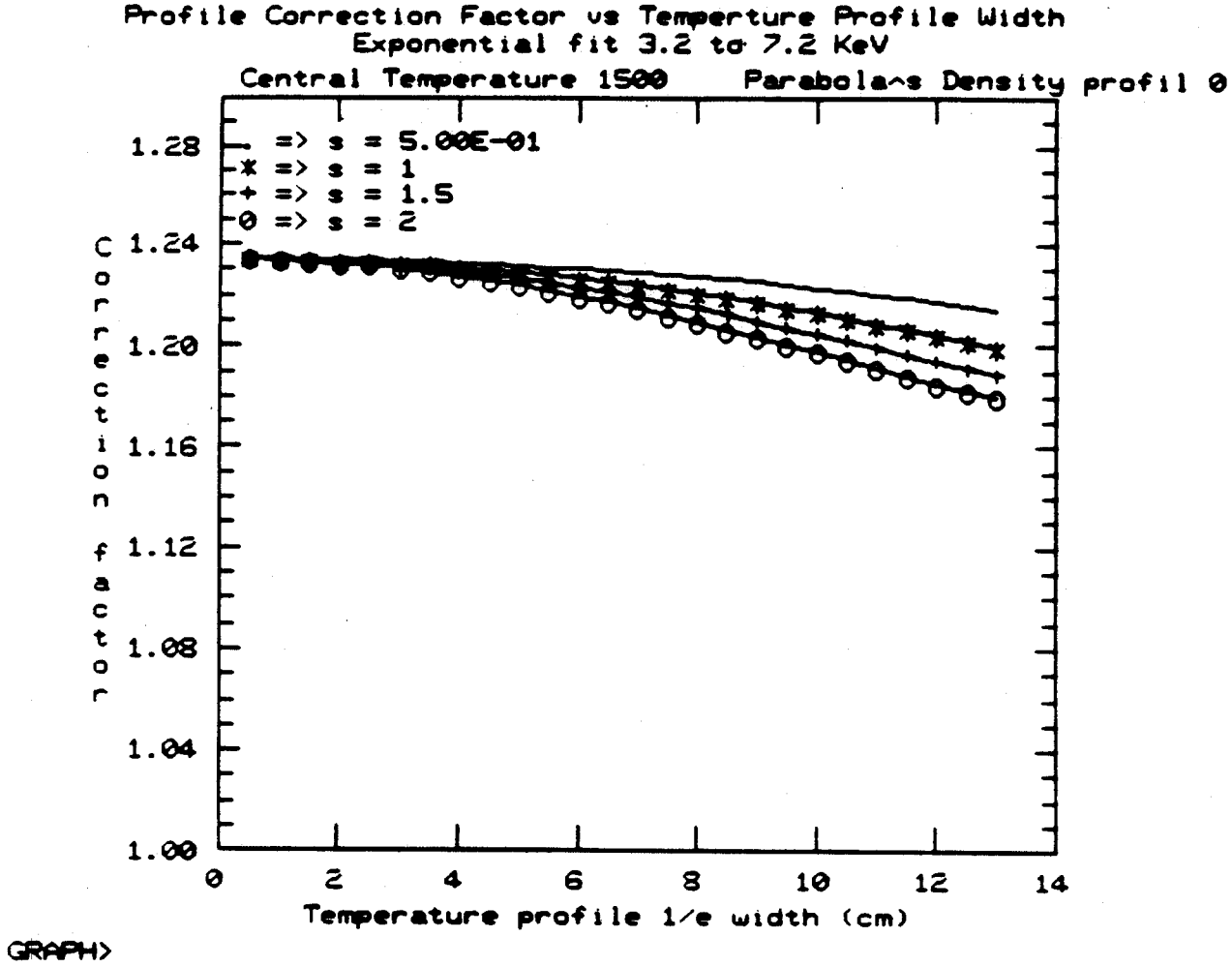

Figure 5
Profile Correction Factor vs Temperature Profile Width

replaced by $g+f_i(T,h\nu)$. For a completely stripped ion,

EQ2 $$f_i = 2\theta_i \sum_{m=m_i(h\nu)}^{\infty} \exp(-\theta_i/n^2) g_n(h\nu)/n^3$$

where n is the quantum number of the final hydrogen-like state, $m_i(h\nu)$ is the lowest quantum number for which emission can occur at energy $h\nu$, $\theta_i = Z_i^2(13.6eV/T_e)$, and $g_n(h\nu)$ is a tabulated function [4].

Figure [6] illustrates the contribution of radiative recombination to the x-ray spectrum with a .17% oxygen contamination in an 870 ev plasma [10]. The net result is a discontinuity at 870 ev (The K-shell ionization potential of oxygen) and an enhancement of the spectral intensity by a factor of 2. Oxygen is completely stripped in plasma regions hotter than 220 eV [11] so the assumption of completely stripped initial states is a good one for most of the plasma volume.

The dominant high-Z impurity in ALCATOR C discharges is molybdenum. It is introduced by circular "limiters" that are placed in the machine at one or more toroidal locations to prevent the plasma from damaging the relatively thin wall of the vacuum chamber. Molybdenum has an L-shell recombination edge at ≈4 KeV. The presence of this edge could affect x-ray electron temperature measurements, since changes in the molybdenum density or electron temperature would cause the intensity of the continuum to change differently above and below the edge. However, extensive searches with various

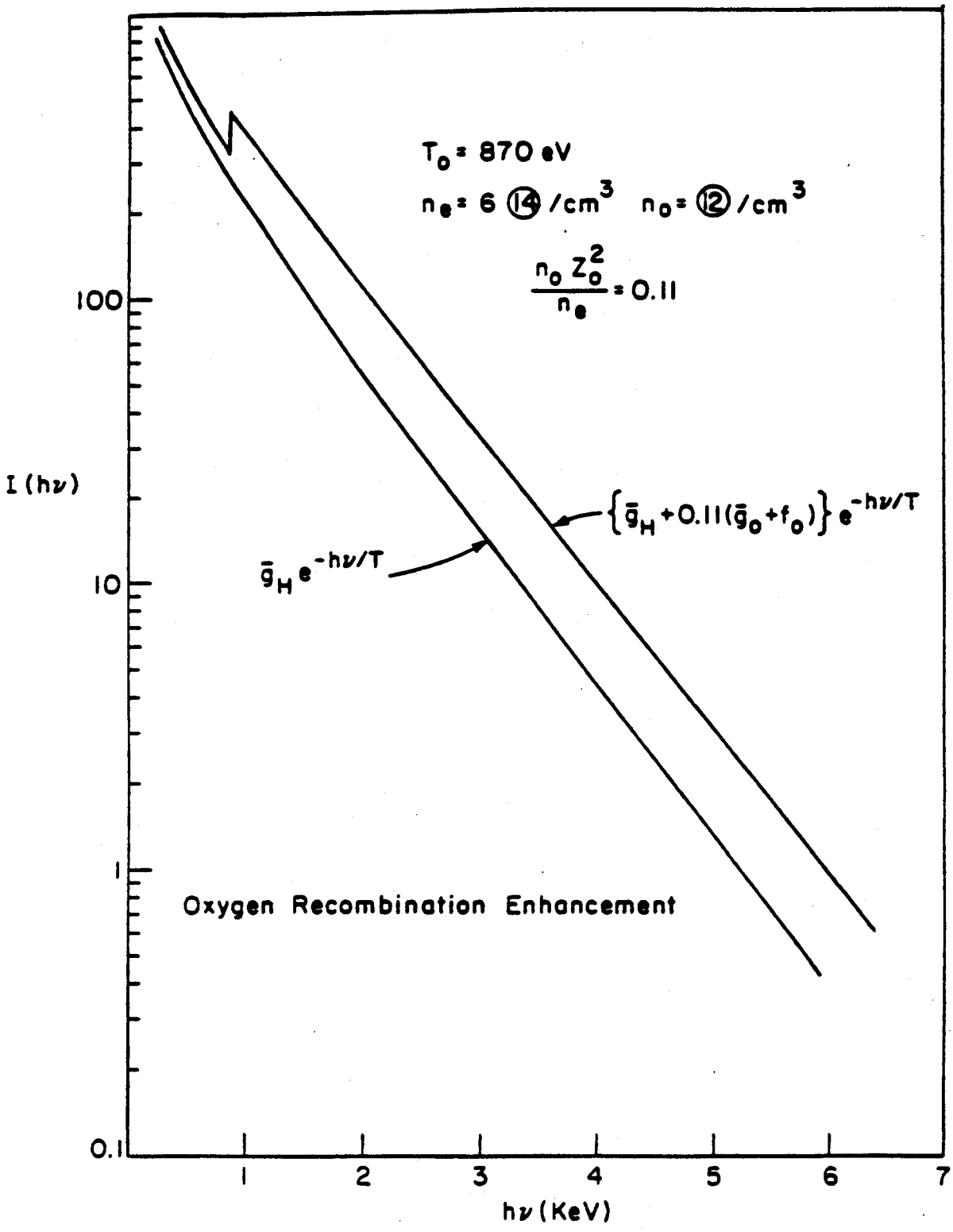

Figure 6
Radiative Recombination

instruments have failed to show a recombination edge in ALCATOR C [12]. Figure [7] shows an x-ray spectrum taken with a Si(Li) detector from a plasma with a very high concentration of Molybdenum. Note that though the Molybdenum L lines dominate the spectrum, no recombination edge is evident. The Molybdenum recombination edge does not strongly influence the X-ray continuum, and since Molybdenum is the dominant high-Z impurity, it is unlikely that any recombination edges are important.

RESONANT TRANSITIONS

Impurity electrons in a hot plasma can undergo resonant transitions from bound states to bound states. The usual result is emission of a photon with energy equal to the difference in energy between the initial and final states. In ALCATOR C plasmas the normal central electron temperature of 1-3 KeV completely strips low-Z impurities of all electrons, and resonant transitions are not likely. Medium and high-Z impurities are only partly stripped, and spectroscopists find an abundance of resonant transition lines in the optical, ultraviolet, and x-ray regions. A complete treatment of impurity line radiation and its effects on the plasma is beyond the scope of this thesis. An excellent review is given by Von Goeller [9]. The importance of impurity lines is that their intensity is not simply related to the electron temperature. Any technique that attempts to determine the

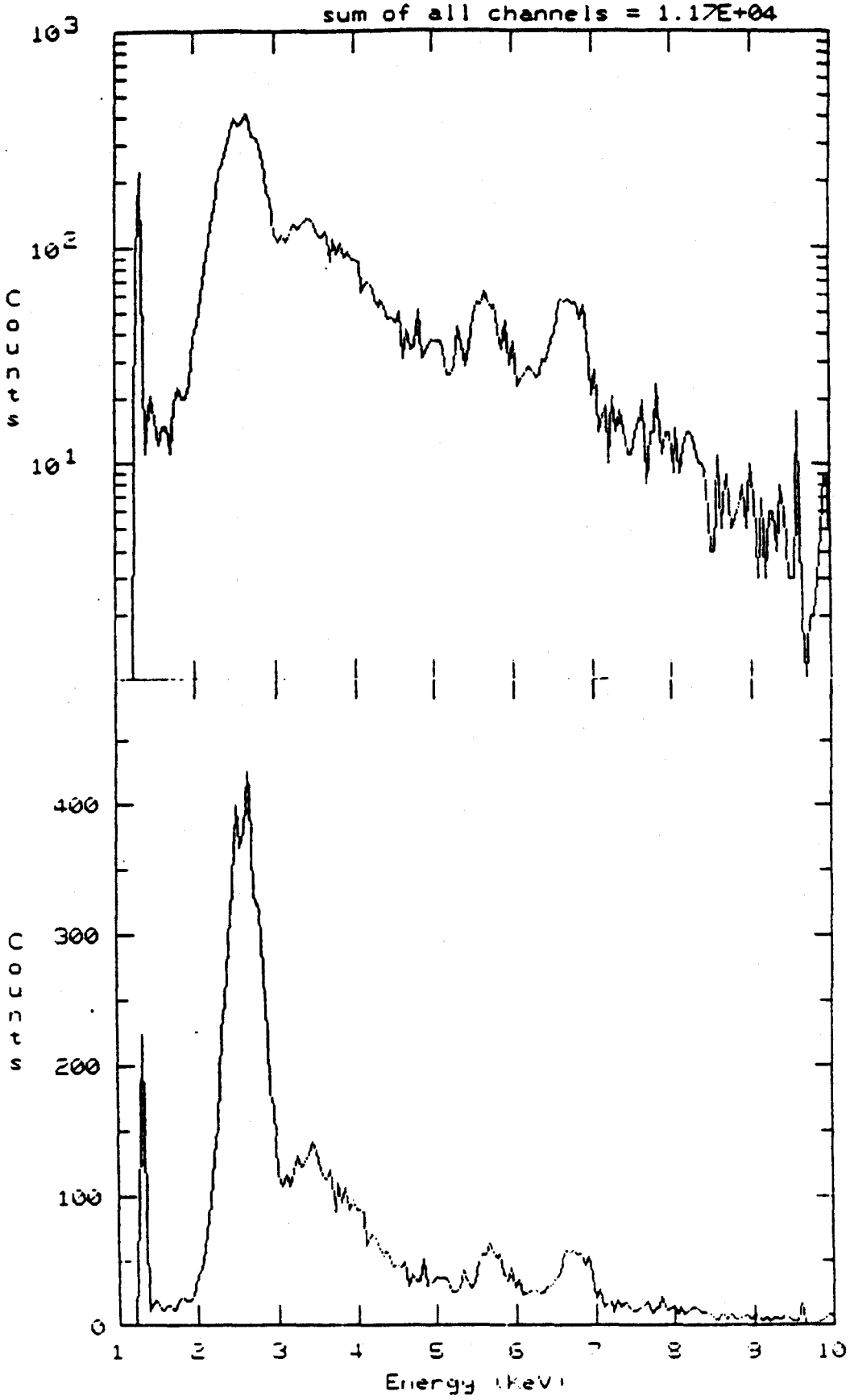

Figure 7
Molybdenum Dominated Si(Li) Spectrum

electron temperature from the x-ray continuum must either use portions of the spectrum that contain no lines or somehow determine the energy and intensity of each line.

Electron Temperature Measurement Techniques

A number of experimental techniques are used to determine the electron temperature in nuclear fusion research plasmas. The probe techniques that are commonly employed in undergraduate physics laboratories are of little use because the hot, dense plasma will quickly destroy any probe.

The characteristic time for the electron distribution function to thermalize is on the order of 10 electron-electron collision times. The electron-electron collision time is roughly a microsecond for ALCATOR plasmas. Diagnostics that complete a temperature measurement in 10 microseconds or less will therefore measure the instantaneous temperature, while diagnostics that require much longer will measure some averaged value of the temperature.

THOMSON SCATTERING

Thomson scattering is a common electron temperature diagnostic [13]. In this technique an intense beam of laser light irradiates the plasma. The electrons in the plasma, moving with thermal velocities of $\approx .05c$, Thomson scatter the photons, changing their wavelength. Photons scattered at some angle, usually 90 degrees, are collected and analyzed by

a spectrometer. The broadening of the laser line width due to the velocity of the electrons can be related to the electron temperature. The intensity of the scattered light proportional to the density of the plasma in the scattering volume.

The chief advantage of Thomson scattering stems from the local nature of the measurement. The spatial resolution of the instrument is ultimately limited by the diameter of the laser beam, which is typically a few mm. The measurement is essentially instantaneous; the laser pulse width is about 10 nsec. The primary disadvantage of Thomson scattering is that it is a rather difficult measurement to make. The Thomson scattering cross section is so small that extremely powerful lasers are required. The most commonly used laser systems are q-switched ruby lasers. Laser outputs of 10 joules in 10 nsec pulses are feasible, giving power levels of 10^9 watts. Even with this enormous flux, only a few hundred or thousand photons are scattered from the volume of interest. Extreme care in the design of the analysis system is required for reasons of both efficiency and stray light. Background corrections for stray plasma light and photomultiplier dark noise are required. A second disadvantage of Thomson scattering is that it cannot be rapidly repeated; the lasing medium cannot be cooled fast enough. There are some systems that can fire a burst of several pulses in a few milliseconds [13], and systems are either working or under development that will pulse continuously at 50 Hz [14],[15]. There have

been proposals for Thomson scattering systems based on continuous argon-ion lasers [16], but there are no working systems to date. A 100 watt laser should provide sufficient signal for a measurement every 10 ms.

ELECTRON CYCLOTRON EMISSION

Electron cyclotron emission (ECE) from the plasma can be used to determine the plasma temperature. A maxwellian electron velocity distribution radiates at the electron cyclotron frequency and its harmonics. If the plasma is optically thick, the intensity of the radiation is proportional to the local electron temperature. The 1/r dependence of the toriodal magnetic field causes all points on a cylinder at a given major radius to radiate at one frequency. A measurement of the electron cyclotron emission spectrum can therefore be used to determine the electron temperature profile. Unfortunately, it is very difficult to absolutely calibrate detectors, antennas, and windows in the millimeter wavelength region where electron cyclotron emission occurs. ECE diagnostics usually rely on some other diagnostic for the absolute value of the electron temperature. The intensity of the emission is strongly influenced by the high-energy electrons, making the instruments very sensitive to non-thermal distribution functions. Non-thermal emission has been observed on a number of Tokamaks, including ALCATOR C [17], [5].

X-RAY CONTINUUM TECHNIQUES

The X-ray spectrum at energies $h\nu > T_e$ is an obvious method of determining the electron temperature. As shown earlier, the slope of the log spectral intensity is inversely proportional to the absolute value of the electron temperature. Two methods are widely used to measure the X-ray spectrum, high-resolution solid-state detectors and foil filters.

The Si(Li) detector is the most common high-resolution solid state instrument. A silicon diode is drifted with lithium to form a P-intrinsic-N diode with a large intrinsic region. The PIN diode is reversed biased to maximize the depletion volume. The diode and the first FET amplifier are cooled to liquid nitrogen temperature in order to maintain the lithium drift, reduce leakage current, and reduce noise. When an X-ray photon is absorbed in the intrinsic region, it produces hole-electron pairs in proportion to the energy of the incoming photon. The induced charges are swept out of the intrinsic region by the large electric field and the resulting current pulse is amplified and shaped before being sent to a pulse-height analyzer. The pulse-height analyzer collects a complete spectrum, including both resonant transition lines and continuum. Typical Si(Li) detectors have energy resolution of 200 eV at 6 KeV.

Silicon detector systems must operate at average count rates of 20 KHz or less. Higher count rates lead to pulse pile-up and spectral distortion. This limitation requires

Si(Li) systems to integrate for 100 msec or more in order to accumulate sufficient counts for an accurate measurement. If there are strong impurity lines present in the spectrum the integration time can be even greater as the system spends a significant amount of time analyzing photons from the resonance transitions, which do not aid in the determination of the electron temperature. Figure [7] shows a Si(Li) spectrum taken from ALCATOR C. Note that though there are over 11,000 counts, all but 1,700 of them are in the Molybdenum lines.

The temperature that is measured with Si(Li) systems is thus an average over both time and space, though the x-ray emission profile is heavily weighted towards the center of the plasma. Despite these limitations, Si(Li) systems are in place on almost every tokamak, being inexpensive, relatively simple to operate, and reliable.

The Mecuric Iodide solid-state X-ray detector has recently become commercially available. The principle of operation is identical to the Si(Li) detector except that the PIN diode is made from HgI and requires no lithium drift. This eliminates the need for liquid nitrogen cooling. These detectors are useful to higher energies than Silicon systems because of the higher Z (and hence greater x-ray absorption coefficient) of the material. Except for these two advantages, the detector is essentially identical to Si(Li) in function.

The x-ray absorption cross section of all elements exhibit sharp decreases near the ionization potentials of each electron shell. These "absorption edges" can change the

x-ray transmission of a thin foil by a factor of ten or more over a relatively narrow energy range. A foil of proper thickness can have peak transmission of 50% with a resolution of about 10%. Silicon surface-barrier diodes, proportional counters, or NaI scintillators are used to detect the transmitted flux. Two or more foil filter/detector combinations can be used to measure the slope of the x-ray spectrum and thus determine the electron temperature. This method has the advantage of fast time response. The tasks of energy discrimination and photon detection are separated, and the primary limit on the time response of the system is the incident x-ray flux. The primary disadvantage arises from the nature of the foil filters. Not all elements are suitable for rolling into the thin foils required for reasonable x-ray transmission, and the central transmission energy and resolution are not adjustable. The common impurities have resonant transitions in or near the passband of some of the filters, so the detected flux can be "contaminated" by line radiation. The type and level of impurities present in the plasma varies widely, and so the foil-filter technique must be used with care. The measurement must be considered tentative unless the the impurity species and densities are well-known.

REQUIREMENTS for a NEW ELECTRON TEMPERATURE DIAGNOSTIC

As tokamaks have grown in size and performance, so has the need for more complete information about the plasmas that they produce. It is impractical to pulse a large, relatively expensive device like ALCATOR C over and over again with the same plasma parameters. Instead, the diagnostics must be designed to make a measurement in one shot, or several measurements per shot. Better understanding of the basic physics governing plasma behavior requires ever more accurate measurements with finer spatial and temporal resolution. The diagnostic array on ALCATOR C is summarized in Table [2]. A brief inspection shows that the central electron temperature is not well resolved. It can be determined once per shot by Thomson scattering (instantaneously) or by HgI or Si(Li) spectroscopy (averaged over ≈400 msec.) While the electron cyclotron emission can determine the relative electron temperature with good time resolution, the ECE diagnostic is better employed to determine the electron temperature profile. Calibration with the absolute value of the central temperature as determined by another diagnostic gives time and space resolved electron temperatures.

A good target for a time-resolving electron temperature measurement is the m=1 "sawtooth" oscillations commonly observed on ALCATOR C and other tokamaks. These perturbations are most obvious on the integrated x-ray flux measured by surface barrier diodes, and the ECE diagnostic has measured

ALCATOR C DIAGNOSTIC CAPABILITIES

Plasma Parameter	Measurement Technique	Resolution Temporal	Resolution Spatial
Loop Voltage	Pick-up Loops	100 μs	NA
Electron Density	FIR Laser Interferometer	10 μs	4 cm
	Thomson Scattering	10 ns	.5 cm
Hard X-ray Emission	NaI(Tl) Detector	50 μs	none
	NaI(Tl) Array	50 μs	2 cm+
Position	Rogowski Coils	50 μs	.3 cm
	X-ray Diode Array	200 μs	.3 cm
Plasma Current	Rogowski Coil	50 μs	NA
Z_{eff}	Visible Continuum	200 μs	1 cm
	Spectroscopic Measurement	5 ms	1 cm
Ion Temperature	Neutral Charge Exchange	50 ms	2 cm
	Neutron Emission Rate	3 ms	peak
	Doppler Broadening	20 ms	2 cm
Electron Temperature	Thomson Scattering	1/shot	.5 cm
	HgI Spectroscopy	1/shot	peak
	Electron Cyclotron	200 μs	1 cm *

NA - Not Applicable
Peak - Measures peak value
+ - Available only with RF heating
* - Relative values only

Table 2

relative temperature changes from 3-20 % of the central value. The period of the oscillation ranges from 1 - 5 msec, with a long linear ramp and an abrupt fall in a few hundred microseconds. To fully resolve the sawtooth waveform would therefore require a time resolution on the order of 20 usec, but 1 msec resolution would be sufficient for interesting measurements on the longer period sawteeth.

Non-thermal velocity distribution functions in the form of high-energy "tails" superimposed on a Maxwellian distribution are frequently observed, particularly at low densities and/or during RF heating of the plasma. A new diagnostic should be able to determine whether or not such a tail is

present, and still be able to measure the bulk electron temperature in the presence of a tail. (ECE diagnostics, which are very sensitive to high-energy electrons, are of little use in determining temperatures when tails arise.)

Some new tokamaks such as TFTR are attempting to circumvent the rate limitations of solid-state systems by installing multiple Si(Li) detectors, amplifiers, and ADC's in parallel. Besides being cumbersome and expensive, such a system would be difficult to fit in the limited port space available on ALCATOR, and would provide time resolution of only about 10 msec.

The fundamental rate limitation of solid-state systems stems from the nature of the detector. The same device does the job of photon detection and energy discrimination. Foil filter techniques separate the two tasks and achieve a large increase in throughput, but foils have inadequate selectivity. Bragg diffraction provides an alternative means of selecting X-ray energies. Bragg diffraction occurs in crystalline structures when the atomic planes coherently scatter a particular x-ray wavelength. The wavelength that is diffracted is given by

EQ 3 $$n\lambda = 2d \sin\theta$$

where n is the order of the diffraction, d is the spacing between the diffraction planes, and θ is the angle of the incident and diffracted radiation. Figure [8] shows the geometry of Bragg diffraction.

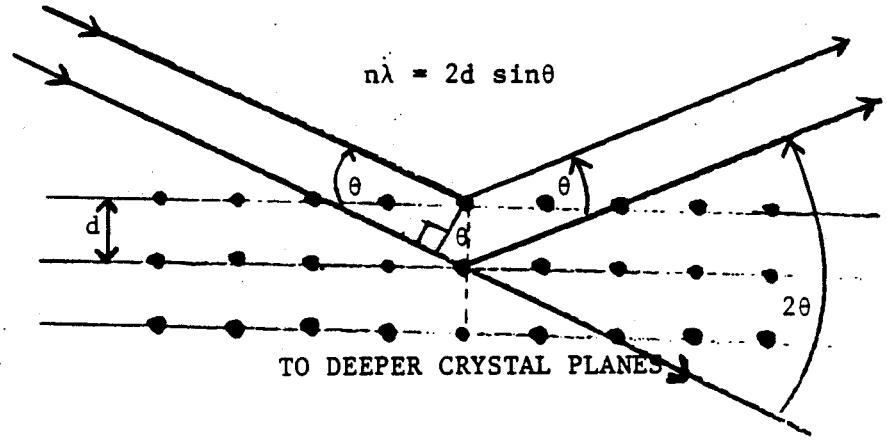

Figure 8
Bragg Diffraction

The details of Bragg diffraction are complex, and the simplified picture given in most college texts is incorrect, since it does not explain why the diffracted radiation is always at the same angle as the incident flux. An excellent explanation is given by Compton [18].

Bragg crystal spectrometers can attain remarkable resolutions, due to the extremely close spacing of the scattering atoms. Resolving powers of 100,000 are not uncommon. Bragg spectrometers of many different geometries are employed on tokamaks to measure impurity spectra. A very high resolution system on ALCATOR C is used to determine the ion temperature by measurement of the doppler broadening of resonant transition lines in selected impurities.

As resolution goes up, continuum flux goes down. An electron temperature diagnostic using Bragg diffraction for energy discrimination requires low resolution in order to collect enough flux for a fast measurement. The resolution of a Bragg diffraction spectrometer is determined by the convolution of the slit function and the resolution of the crystal used. The slit function is roughly triangular with an angular half-width of [19]

EQ 4 $$\theta_s = \mathrm{Tan}^{-1}(s/l)$$

where s is the width of the slit and l the distance between the front and rear slits. The crystal resolution is determined primarily by the degree of crystal perfection. Some materials, such as quartz, can be almost perfect single crystals, while others have many small crystal domains. The degree to which the domains are aligned determines the crystal resolution. These "imperfect" crystals tend to be more efficient diffracting elements than perfect crystals. The alignment of the domains in many imperfect crystals approximate a gaussian curve. The convolution of the slit function and the crystal function will have a half width [19] of

EQ 5 $$\theta = \left(\theta_c^2 + \theta_s^2\right)^{1/2}$$

Where θ_c and θ_s are the crystal and slit angular resolutions, respectively.

The size of the slits is easily varied but ultimately limited by the required spatial resolution. It is therefore

important to select a low-resolution crystal to achieve the highest throughput. It is equally important that the crystal be relatively efficient. Given these two requirements, the best crystal for this application is graphite. Union Carbide Corporation Carbon Products Division manufactures a graphite quasi-crystal for x-ray and neutron diffraction purposes. Normal graphite is nearly isotropic, but the crystal domains may be partially aligned with a hot pressing process. These crystal have the highest integrated reflectivity of any available. The resolution is fairly low, and can be varied by changing the parameters of the pressing process. The crystals selected had angular resolutions of roughly .8 degrees. The efficiency of diffraction varies with energy from 8% at 3 KeV to nearly 25% at 10 KeV [20], [27].

The placement of the channel energy is dictated by the impurity line radiation. It would be impossible to avoid every possible line from every possible impurity, so the channel energies were picked to exclude the most commonly observed impurities, using high-resolution spectra taken with a Bragg monochrometer over a wide range of ALCATOR plasmas. The channels were chosen with approximately equal energy spacing. A graph showing the common impurity lines and the placement and resolution of each channel is shown in figure [9].

The x-ray detector must also be chosen with care. The detector must be capable of handling input rates of up to 10 MHz, and must be relatively efficient. A desirable but not

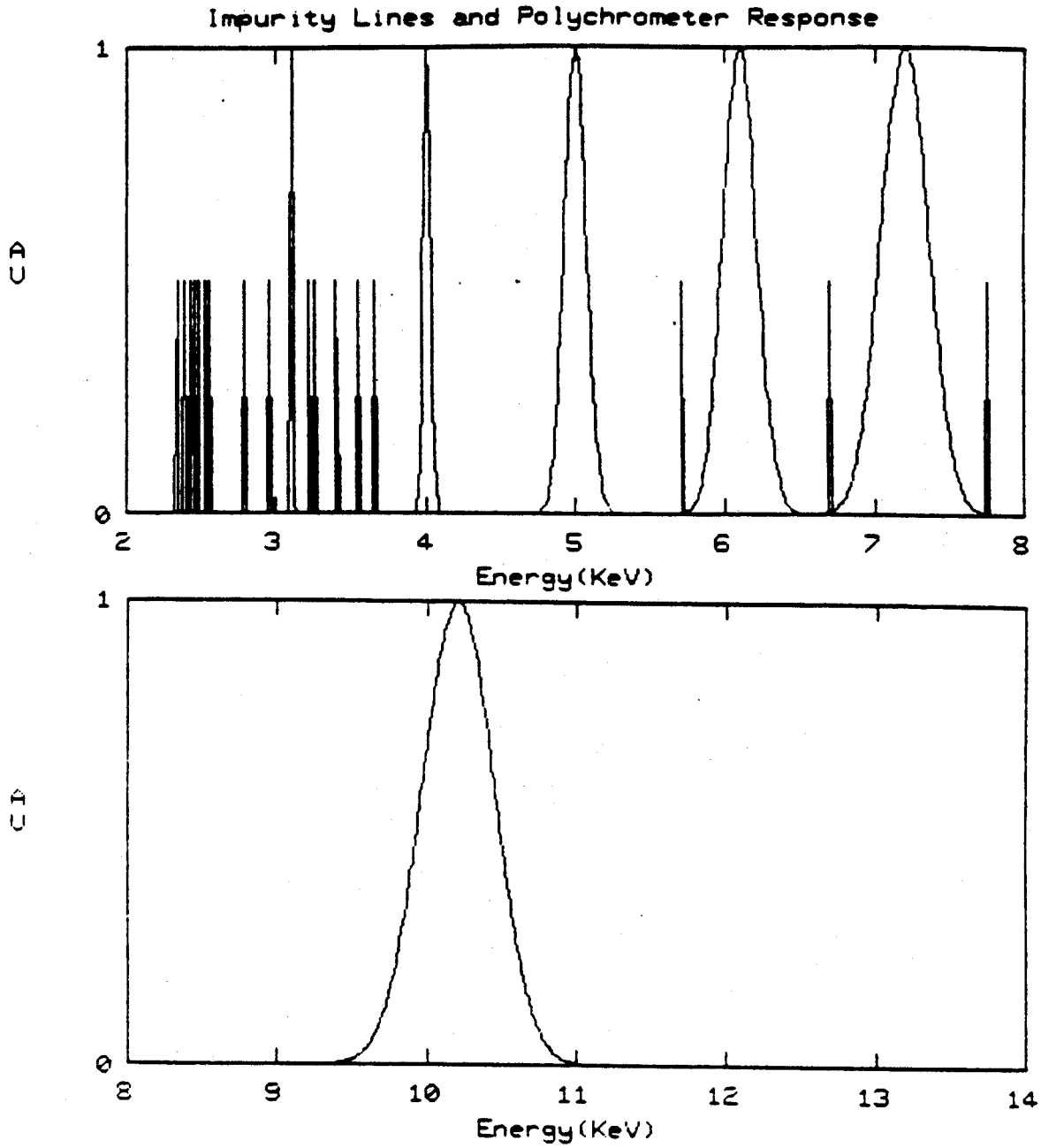

Line	Energy	Line	Energy	Line	Energy
Si^{13+}	2.01	Mo^{25+}	2.56	Mo^{32+}	3.40
Mo^{17+}	2.34	Mo^{31+}	2.67	Cl^{16+}	3.54
Mo^{22+}	2.39	Cl^{15+}	2.79	Mo^{32+}	3.65
Mo^{23+}	2.43	Cl^{16+}	2.95	Cr^{22+}	5.71
Mo^{25+}	2.46	Mo^{32+}	3.22	Fe^{24+}	6.70
Mo^{22+}	2.48	Cl^{15+}	3.26	Ni^{26+}	7.75
Mo^{23+}	2.53	Mo^{32+}	3.31		

Figure 9
Commonly Observed Impurity Line Transitions with Placement and Resolution of Each Channel

essential quality is the ability to resolve each x-ray photon, since operation in a pulse-counting mode tends to be less sensitive to slight variations in detector gain.

Plastics doped with various phosphors are used as nuclear radiation detectors, but they are not efficient at the relatively low energies involved in this experiment. Proportional counters exhibit serious gain variation at count rates in excess of 100 KHz. Surface barrier diodes are efficient detectors but have no intrinsic gain. The maximum count rates expected in this experiment would be barely detectable with a standard SBD. Thallium activated Sodium Iodide, the first commonly used scintillator, is also the one of most efficient. It converts 13% of the incident x-ray's energy into blue photons with an energy of 3 ev [21]. The scintillation is characterized by several time constants, the shortest being 250 nsec. This is a rather long time constant for pulse counting at 10 MHz, but the average light level can be measured. About 7-9% of the light is emitted with a time constant of 150 msec [21],[22], and this fluorescence must be accounted for in order to make accurate measurements at high count rates.

There is one faster, more efficient scintillator available. Pure sodium iodide has not found much use because it must be cooled to liquid nitrogen temperatures to become efficient. At that temperature, it is nearly twice as efficient as NaI(Tl), and most of the light is emitted with a time constant of 60 ns [21]. Unfortunately, fiber-optic light

guides do not work well at liquid nitrogen temperatures. The index of refraction of the cladding material changes and the transmission efficiency is drastically reduced. There are available rather expensive fibers that use a fluorine-doped quartz as cladding and are suitable for use at low temperatures, but they collect only 1/4 the light that the best room-temperature fibers will. The scintillation is at a wavelength of 300 nm, where quartz fiber is less transparent and photocathodes less efficient than at 410 nm. For reasons of simplicity and signal strength NaI(Tl) was selected as the scintillator material.

ALCATOR produces x-rays with energies up to 1 MeV, from high-energy electrons and ions colliding with the limiters and from D-D fusion neutrons scattering in the magnet and room. It is important to keep the detectors relatively insensitive to this flux. The detectors were chosen to be as thin as the manufacturer would handle in order to reduce the hard x-ray detection cross-section. The detectors selected have 50% probability of stopping a 100 KeV photon.

The amount of x-ray flux that can be collected from ALCATOR C is limited by the access to the plasma. The widest flanges are only 1.65 inches across, and all but 4 are narrower. It is impractical to place the spectrometers inside this "keyhole" for several reasons other than the cramped quarters. The ambient temperature is 77 degrees Kelvin because the flange is cooled, along with the toroidal field magnet, with liquid nitrogen. The toroidal field magnet

partially encloses the flange and the magnetic field can reach 10 Tesla. The radiation and particle flux from the plasma can reach 10 W/cm^2, high enough to damage the thin Beryllium foils used to isolate the instrument from the ALCATOR vacuum system.

Locating the instrument just outside the "keyhole" puts it approximately 45 cm from the plasma center. Once the distance from the plasma is known, it is possible to calculate the expected x-ray flux for a given set of plasma parameters. The flux is given by:

EQ 6
$$F(h\nu) = 2.4\times10^{-16}\left(\Delta h\nu/h\nu\right)\Delta A\Delta\Omega \times \int dl\ n_e^{\,2}(l)\,\zeta(l)\,\bar{g}(l)\sqrt{T_e(l)}\,e^{-h\nu/kT(l)} \quad \text{photons/cm}^2\text{-sec}$$

where $\Delta h\nu$ is the energy resolution, T_e and n_e are the plasma electron temperature and density respectively, and ζ is the enhancement of the continuum due to recombination. The integral is carried out along the chord viewed by the instrument. The flux is used to determine the required size of the entrance window for each channel in order to achieve the desired time resolution. The expected flux can vary considerably if large enough extremes in plasma parameters are included. The value of ζ is not well known but it varies with plasma density and is typically between 2 and 50 [23]. At low densities, when the plasma is usually hot, the molybdenum density rises and ζ rises as well. At high densities the molybdenum concentration and plasma temperature

tend to be lower, and ζ is lower. This variation in ζ is helpful because it tends to counteract the n^2 dependence of the x-ray flux and reduce the dynamic range required of the polychrometer.

The terms $\Delta A \Delta\Omega$ represent the area of the plasma viewed and the solid angle subtended by the detector. It can be shown [24] that for an extended source,

EQ 7 $$\Delta A \Delta\Omega = A^2/l_{12}^2$$

where A is the area of the front and back slits (assuming both slits are the same size) and l_{12} is the distance between the slits. The approximation that the plasma is an extended source is valid only if the instrument is viewing a small enough region that the temperature and density are relatively constant. For the 32-cm diameter ALCATOR plasma, 1.5 cm spatial resolution was chosen as a compromise between good spatial resolution and high flux.

Now that the spatial resolution and emission from the plasma are known, the collection area required to achieve peak counting rates of order 10 MHz can be calculated. The expected counting rate is

EQ 8 $$R_d = \eta_d \eta_c F(n_e, T_e, \zeta)$$

where η_c is the efficiency of the crystal diffraction, η_d is the detector efficiency, and F is the integrated plama flux as given above. It would be possible to select a different area for each channel so that the flux rates would be roughly

the same in all channels at a given temperature, but for the sake of design simplicity this was not done. The energy resolution of the channels decreases with increasing energy, as demonstrated by taking the derivative of the Bragg law and converting wavelengths to energy.

The results of the above calculations are displayed in Table [3] for three plasma conditions. Based upon the results of calculations such as those displayed in Table [3], the collection area was chosen to be 0.6 cm^2. This allowed room for up to 7 channels, each 1 cm x .6 cm.

EXPECTED COUNT RATES IN EACH MONOCHROMETER CHANNEL
for THREE TYPICAL PLASMA CONDITIONS

Energy (eV)	3100	4200	5000	6100	7200	10200
Case 1	3.3×10^6	3.8×10^6	4.4×10^6	3.8×10^6	2.9×10^6	7.5×10^5
Case 2	6.0×10^6	5.4×10^6	5.0×10^6	3.0×10^6	1.7×10^6	2.0×10^5
Case 3	6.5×10^6	5.0×10^6	4.0×10^6	2.0×10^6	9.7×10^5	6.7×10^5

Table 3

The first entry represents the expected flux rates per sq cm of collection area for a plasma with T_e=2500 eV, $n_e = 1.5\times10^{14}$, and $\zeta = 6$. This is at the low end of normal ALCATOR densities. The second entry is a more typical plasma with $n_e = 5\times10^{14}$, T_e = 1500 eV, and $\zeta = 2.5$. The last entry represents the plasma shortly after fueling by ablation of a solid pellet of frozen hydrogen injected at high speed in the machine. Such a plasma has a more sharply peaked density profile, described by a parabola[2]. The temperature is 1200 eV at a density of 8×10^{14} with a ζ of 2.

Description of the Instrument

A schematic drawing of one channel of the polychometer is shown in Figure [10]. X-rays emitted from the plasma pass through a 10mm x 6mm x .025 mm Be window, which serves to isolate the instrument from the ALCATOR vacuum system. The x-rays pass through a collimator contructed from a piece of jet turbine blade seal manufactured by VAC-HYDE of Danvers, MA. It consists of layers of .1 mm inconel crimped and brazed together to form a honeycomb structure. Each cell of the honeycomb is 1.6 mm across the faces and 50 mm long. The entire collimator is 44.5 mm wide and 25 mm tall. The spatial resolution of the collimator 45 cm from the plasma is 1.5 cm. X-rays emerging from the collimator have an angular divergence of 0.8 degrees.

After collimation, the x-rays impinge upon graphite crystals held at predetermined angles by machined stainless steel wedges. The angle of each wedge was machined to an accuracy of 5 minutes of arc. The graphite crystals are cemented to stainless steel holders that have ground parallel faces. All of the crystals are 6mm wide, 37mm long, and 1mm thick. They were donated by Richard Bleach and David Nagel at the Naval Research Laboratory. The crystals are identical and the holders are designed so that any crystal may be used in any of the 6 channels. The 2 highest energy channels are at such a shallow angle that 2 crystals are placed end-to-end in order to intercept all of the incident flux.

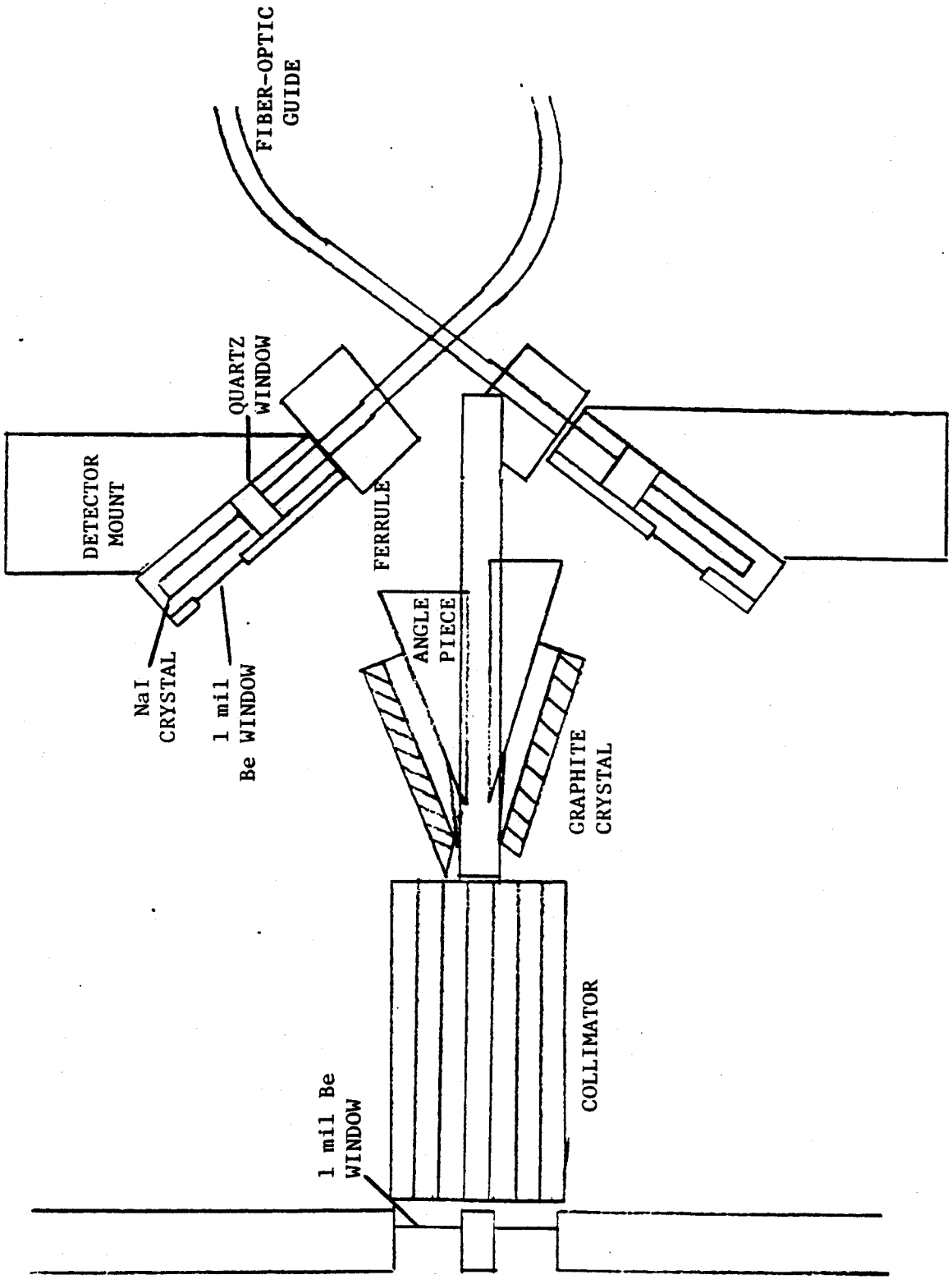

Figure 10
Schematic Drawing of the Instrument

After diffraction by the graphite crystals, the x-ray flux in each channel is intercepted by a NaI(Tl) detector. Each detector has a 4 x 8 x 0.25 mm Be window. (The detectors were designed with 6 x 10 mm windows, but the manufacturer, Harshaw Chemical Co, occluded subtantial parts of each window with epoxy.) Each NaI(Tl) crystal is 12 x 8 mm x 2 mm and is optically coupled to a quartz window. The crystals are packed on 4 sides (those not facing either window) with a reflective material to improve the light collection efficiency.

The scintillation pulses produced by the detector are carried out of the ALCATOR C port (where the ambient temperature is near 77 degrees Kelvin and the magnetic fields can exceed 3 Tesla) on quartz fiber-optic light guides. The guides are 2 m in length and designed for high coupling and transmission efficiency at the scintillation wavelength of 410 nm. Each light guide has a stainless steel ferule near the center of the assembly to form a vacuum seal. The light pipes were manufactured by Fiberguide Inc, of Stirling, NJ.

The entire assembly was located in a vacuum chamber to eliminate the attenuation of soft X-rays by air. The chamber was constructed of a 40 cm diameter stainless steel tube. The tube also served as a re-entrant port to bring the entrance windows as close to the plasma as possible. The X-ray entrance windows were located at one end of the tube, and the fiber-optic guides penetrated the opposite end. A compound to match the index of refraction was not employed at the detector end of the light guides because experience showed

that the coupling compound would bubble under vacuum and drastically reduce the coupling efficiency. Matching compounds were used at the photomultiplier end of each guide. The photomultipliers were variations on the standard 1p28 type with a quartz envelope to improve transmission at 400nm. The photomultipliers have a quantum efficiency of 20% at 410 nm, a current gain of 10^6, and an anode pulse rise time of 15 nsec.

The photomultiplier output was fed into a 20 kΩ resistor, and the resultant signal buffered by a LM301 unity-gain follower with a bandwidth of 20 MHz. The follower outputs were then fed into the pulse analysis circuitry. Two type of analysis circuitry were employed, counting mode and current mode.

The counting mode circuitry, shown in Figure [11], begins with an array of 200-MHz direct coupled linear amplifiers made by Lecroy Research. Each amplifier has adjustable gain from 4 to 40. The output of each amplifier feeds a 100 MHz discriminator, which produces an adjustable-length ECL output pulse whenever the input exceeds the threshold set via a front-panel adjustment. The output of each discriminator is routed to a Lecroy 8212 scaler. The scaler counts the discriminator pulses until a latch signal is received, when it stores the summed count in a buffer, resets the counter, and resumes counting. The "dead time," during which the scaler will not count input pulses, is less than 100ns. The time between latch pulses is used to store the number in each

buffer in an external memory. The external memory is read into a Digital Equipment Corp. VAX-11/780 minicomputer over a CAMAC (IEEE 583) serial highway. The latch pulses are generated by a Lecroy 8501 clock, which can be programed over the CAMAC highway to produce a given number of pulses at a selected frequency upon receipt of a trigger signal. The trigger signal was provided by the ALCATOR control system sequencer 30 ms before the initiation of each discharge.

The current mode circuitry, shown in figure [12], starts with linear amplifiers and anti-aliasing filters. Six channels of a LeCroy 8212 32-channel A/D converter were used to sample the average output current of the PMT at 5 Khz. The sampled values were stored in an external memory and read into the VAX via the CAMAC highway.

RELATIVE ADVANTAGES OF ANALOG AND COUNTING MODES

The two modes of operation have distinct differences. Counting mode has the advantage of being relatively stable to minor variations in PMT gain or fiber optic coupling efficiency. Counting mode is also not sensitive to the 150 msec flouresence of the NaI scintilator, and counts any hard x-rays that stop in the scintilator as one pulse. Analog mode is not subject to pile-up and allows for the use of anti-aliasing filters. Counting mode cannot utilize anti-aliasing filters becase each pulse is either detected or not; no filtering is possible. The only method of reducing alias-

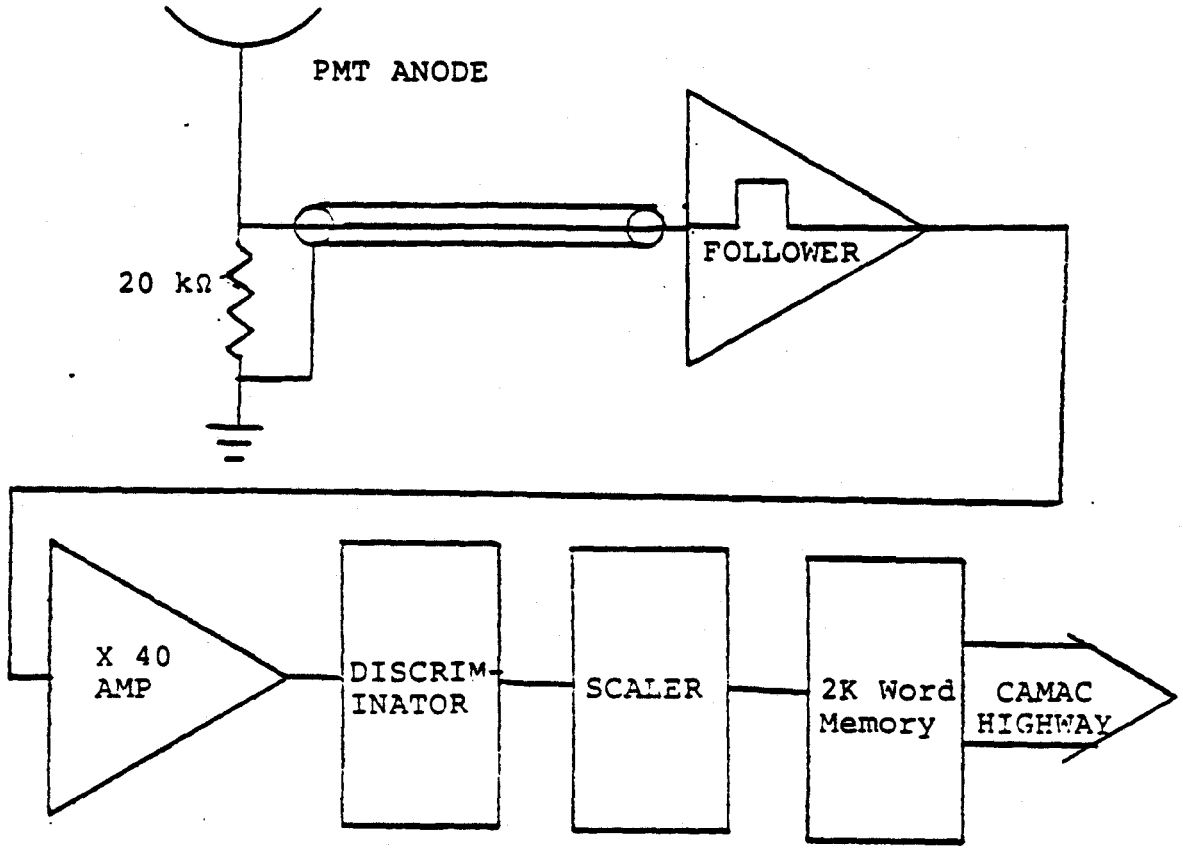

Figure 11
Count Mode Circuitry

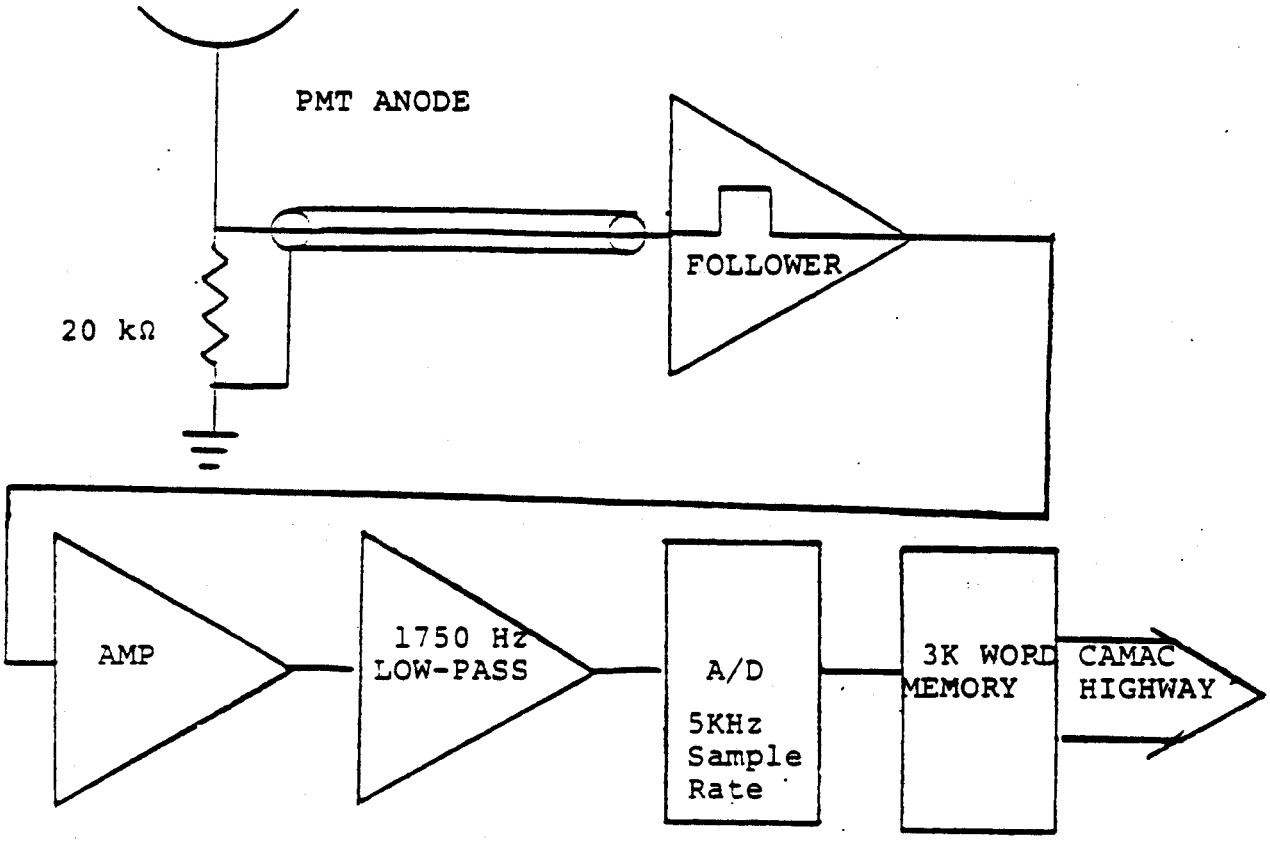

Figure 12
Current Mode Circuitry

ing in counting mode is to stobe the latch signal faster. While analog mode does not have the same dynamic range as counting mode, the overall sensitivity of a channel may be easily changed by adjusting the bias on the PMT. A summary of the differences in the two modes is presented in figure [13].

ANALOG MODE	COUNTING MODE
Sensitive to variations in PMT gain and fiber coupling efficiency.	Insensitive to variations in PMT gain and fiber coupling efficiency.
Anti-aliasing filter desireable.	Anti-aliasing filter impossible
Weights hard X-rays by energy.	Counts hard X-rays as 1 photon.
Not subject to pile-up.	Subject to pile-up.
Sensitive to NaI afterglow.	Insensitive to NaI afterglow.
Dynamic range limited by digitizer to 4000.	Dynamic range limited by counting electronics to about 1,000,000.
Sensitivity can be easily varied.	Sensitivity is hard to vary.

Figure 13
Relative Advantages of Counting Mode and Current Mode

RESULTS

The assembled instrument was first checked to insure that each channel had the anticipated central energy and resolution. Bremsstrahlung radiation from a Cu-anode x-ray tube was collimated by a single tube of the collimator. It was impossible to use the entire collimator because the x-ray source beam was 3 mm in diameter. A Si(Li) spectrometer was used in place of the NaI detector. The resulting spectrum was analyzed to determine the central energy and resolution. The 3.1 and 4.1 KeV channels have resolution much higher than the Si(Li) detector, so only the central energy could be determined. The results of the measurement are shown in Table [4]. The results are very close to the predicted values. One crystal was found to have a .4 degree error; it was discarded.

The x-ray polychrometer must be placed as close to the plasma as possible in order to maximize the x-ray flux. This requires a re-entrant tube that places the instrument 45 cm from the plasma center. A drawing of the ALCATOR port with the reentrant tube is shown in figure [14]. Unfortunately, when the re-entrant tube was first inserted into the vacuum chamber on Dec 5, 1983, it did not fit. Port space and run time are precious commodities on ALCATOR C, so the entrance window was installed without the reentrant tube while the tube was modified. This resulted in lower flux and degraded spatial resolution, but allowed for initial check-out and testing of the system. The modified tube was installed on ALCATOR on December 12, 1983.

PREDICTED AND MEASURED CENTRAL ENERGY AND RESOLUTION
of Each Monochometer Channel

Channel Number	Central Energy		Resolution	
	Predicted	Measured	Predicted	Measured
1	3100 eV	3110 eV	30 eV	---
2	4000	3995	102	---
3	5000	4960	307	300
4	6100	6120	469	460
5	7200	7300	664	650
6	10200	10050	1000	950

Table 4
The resolution of the two lowest energy channels was too fine to be measured with a Si(Li) spectrometer

Counting Mode Operation

In counting mode, scintillator pulses from each diffracted x-ray photon are counted for a pre-determined time and stored in a memory, with 2048 memory locations available for each channel. ALCATOR plasmas typically last 500-800 msec, so a collection period of .5 msec was used to insure that the entire plasma history would be recorded. The clock was started 30 msec prior to initiation of the plasma in order to check for noise and determine the background count rate in each channel. The background varied from channel to channel, but was less than 20 counts/millisecond for all channels.

Determination of the electron temperature requires that the relative sensitivity of each channel be known. It is

4535

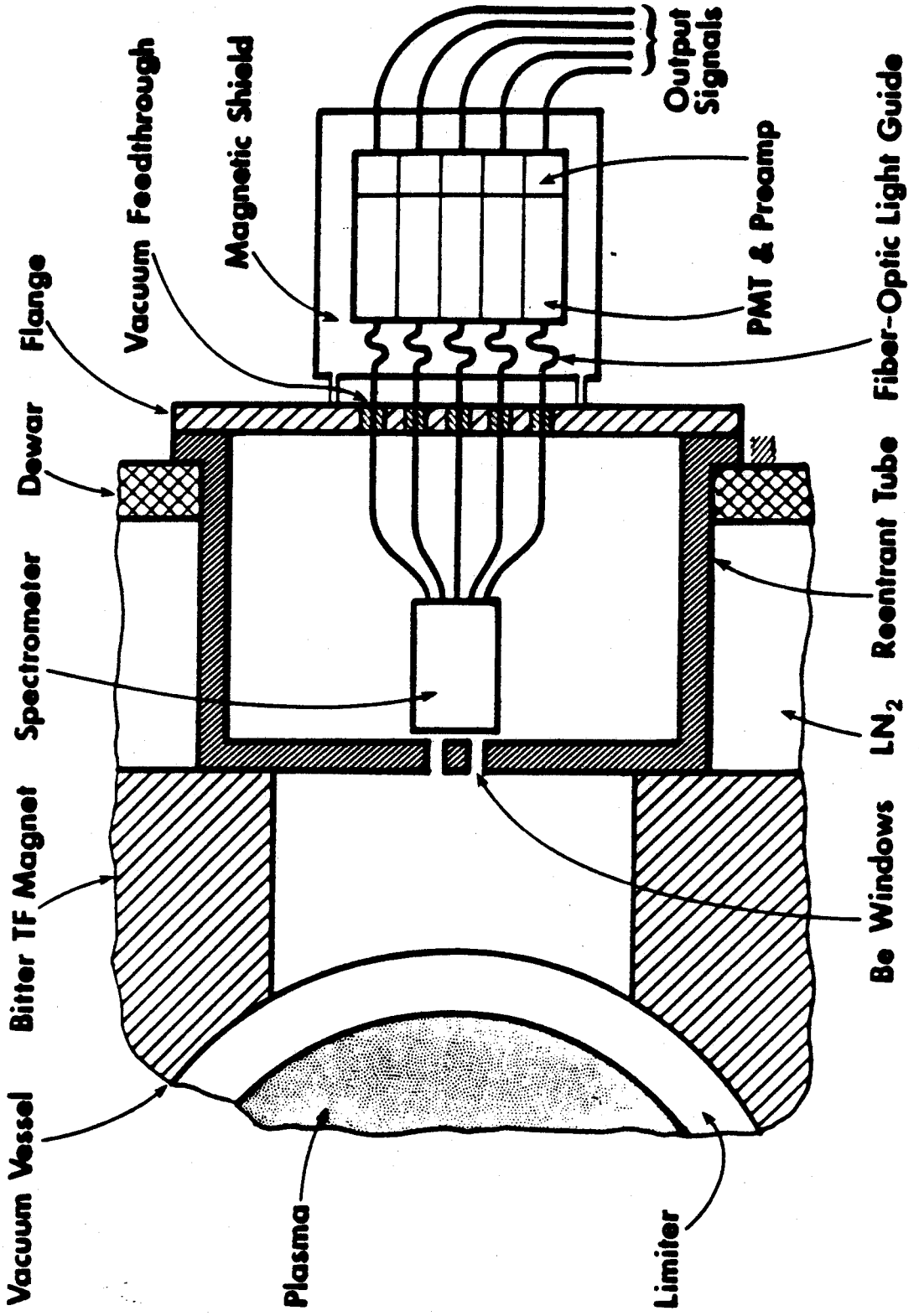

Figure 14
ALCATOR Port Showing Re-entrant Tube and Spectrometer

difficult to calibrate the channels in the laboratory because spatially extended x-ray sources of sufficient intensity and energy were not readily available. A standard isotope source does not produce much continuum radiation, and x-ray tubes tend to be point-like sources. Calibration was therefore performed on ALCATOR. A standard HgI detector system was used to measure the electron temperature of the plasma during a period when the density and temperature was assumed to be relatively constant. The temperature was measured by fitting an exponential to the observed spectrum in the region from 10 to 20 KeV. Relatively small profile correction factors were used to give an estimate of the central electron temperature. This central temperature was then used to determine the temperature that the x-ray polychomator should obseve with profile effects taken into account. Because the polychomator measures the x-ray spectrum at lower energies than the HgI system, the profile correction factor used was larger than the one used for the HgI measurement. The x-ray polychrometer signals were summed over the same collection period as the HgI measurement, and the relative sensitivity of each channel was calculated to make the polychrometer signals correspond to the expected temperature.

Once calibrated, data reduction proceeded as follows. The count in each channel for a given time was divided by the relative sensitivity. The natural logarithms of the resulting numbers were fit to a line by the method of least squares, with proper weighting for the number of counts observed [25].

The inverse slope of the fitted line then gave the profile-averaged electron temperature at that point in time. The quadratic approximation for profile correction shown in figure [4] was applied to yield the central electron temperature. Many shots had count rates of 500 Khz or less, giving only 250 counts in .5 msec. Statistical variation in such small numbers would degrade the precision of the measurement. It would be possible to add groups of channels together to give better statistics, but only at the expense of time resolution. As a compromise, a moving sum was applied to the data before reduction. Typically 5-11 points were summed together.

The results from the counting mode experiments were generally favorable. As a first check of the calibration procedure, the calibration shot was reduced and the temperature averaged over the same period as that used by the HgI system measurement. The average always agreed to within 1% or less. As a second check, later shots were compared with the results of the HgI measurements, and again the agreement was exceptionally good.

A typical discharge is shown in Figure [15]. The plasma current lasts for 550 milliseconds and reaches a peak of 650 KA. The plasma density rises to 2×10^{14} cm^{-3}. From 150 ms to 350 ms the plasma conditions are relatively constant, as evidenced by the integrated soft x-ray flux measured by a surface barrier diode. This portion of the discharge is measured by the HgI system. The counts recorded in each channel are shown in figure [16]. The peak count rate is 400/.5 msec, 800 KHz. The 10.2 KeV channel does not show much

variation. This is probably due to misalignment of the crystal/detector combination or poor coupling between the detector and the fiber optic guide. Whatever the reason, the signal clearly has little to do with the plasma and was not used in the reduction.

The results from shot 30 are shown in Figure [17]. A moving sum of 5 points was used before fitting. Also shown is the goodness-of-fit parameter, r^2, and the 1-σ error estimates in typical fits. The error takes into account only statistical uncertainties and the fitting confidence, with no estimate of the uncertainty in the relative sensitivity of each channel. The fit is very good over most of the discharge. The electron temperature is indeed relatively constant during a substantial portion of the discharge. The average of the electron temperature over this period is 1462 eV, compared to a calibration temperature of 1480 eV.

A more interesting shot, and a more exacting test of the instrument, is shown in figure [18]. In this discharge there were multiple disruptions of the plasma current early in the shot, followed by a sharp increase in plasma current (and Ohmic heating power) later. The soft and hard x-ray traces show a great deal of early activity and become quieter as the shot approaches normal conditions. The polychrometer flux is shown in figure [19]. There is a very high flux rate early, possibly due to impurity recombination enhancement of the x-ray continuum. The temperature is shown in figure [20]. It starts off low and climbs up to a rather high level. The

fit is good over most of the discharge. The calibration from shot 30 was used in reduction. It is noteworthy that the instrument gives consistent results even when the temperature is different than the calibration temperature.

There were some problems with counting mode. The worst problem became apparent when the re-entrant tube was installed and the instrument moved substantially closer to the plasma. The count rate from a typical shot is shown in figure [21]. The count rate exhibits symptoms of counting circuit paralysis as the rate increases beyond 1 MHz. The decrease in observed count rate can be explained by the dc-coupled nature of the counting electronics. At high count rates, the signal from the PMT will not have returned to zero before the arrival of the next pulse. The pulses will overlap, and if the average level of the PMT signal approaches the threshold of the discriminator, the discriminator will not reset and no count will be generated. An extreme example of paralysis is shown in figure [22], where the observed count rate is zero except at the beginning and end of the discharge. Further discussion of counting circuit paralysis and pile-up is reserved until later.

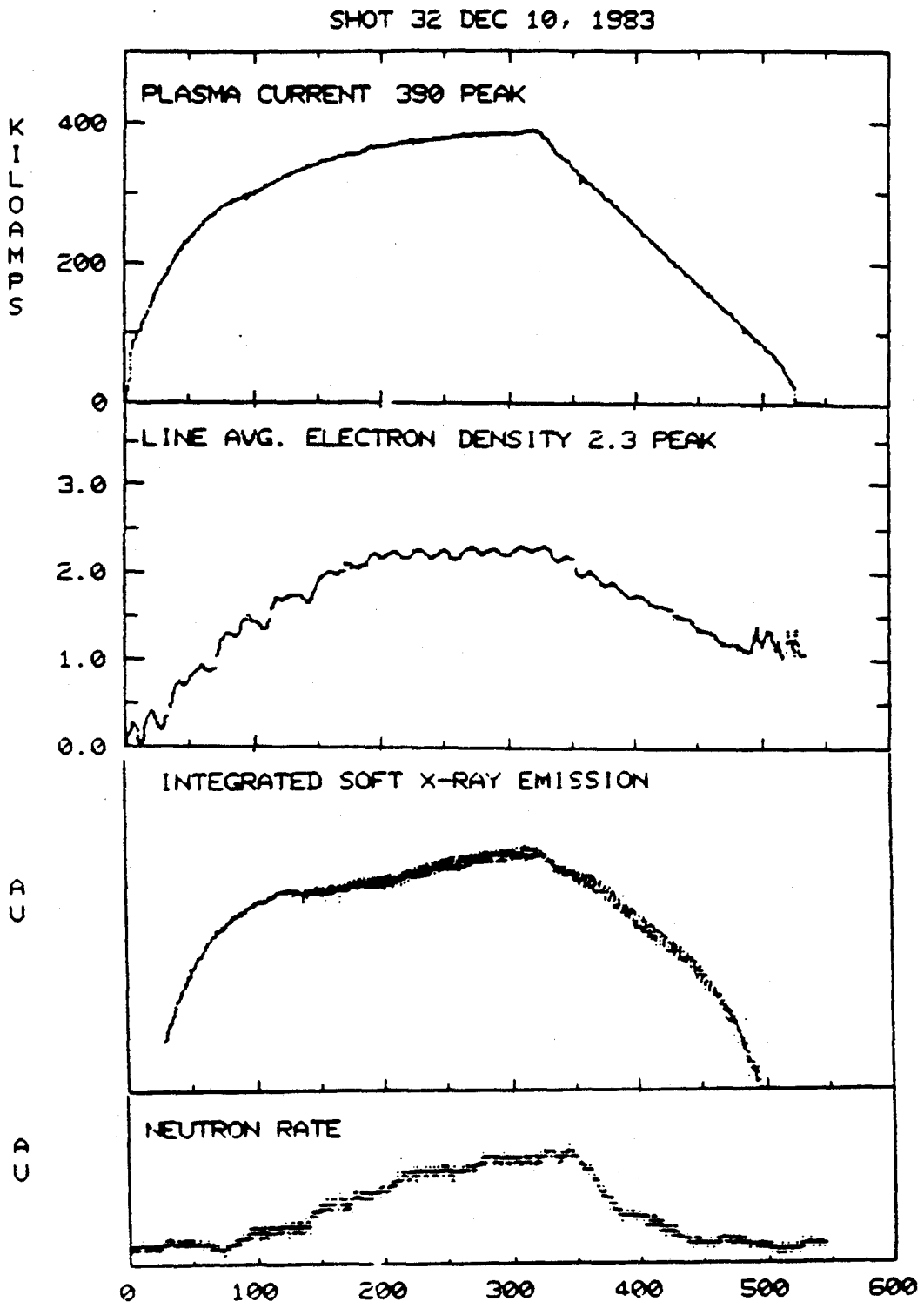

Figure 15
Plasma Current, Electron Density
Soft X-ray Flux and Neutron Rate
Discharge #32 on December 10, 1983

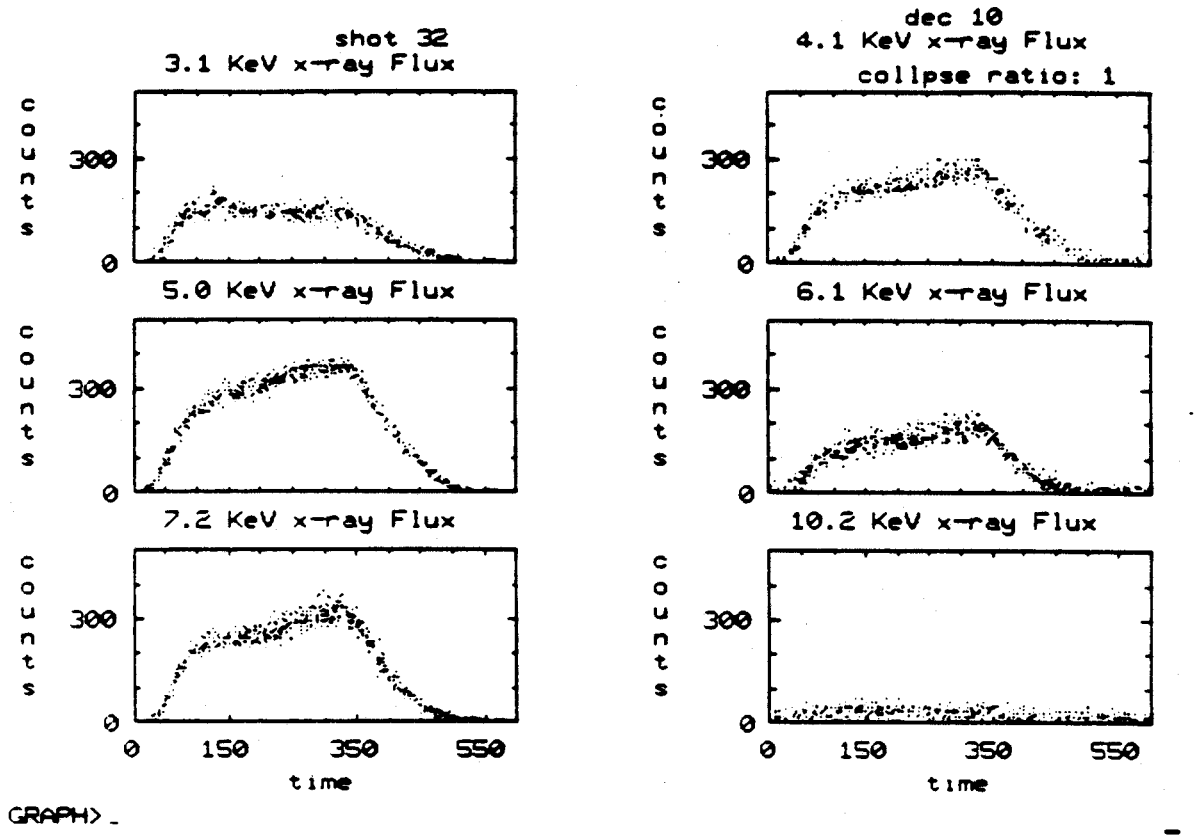

Figure 16
X-ray Flux in Each Monochrometer Channel vs Time
Discharge #32 on December 10, 1983

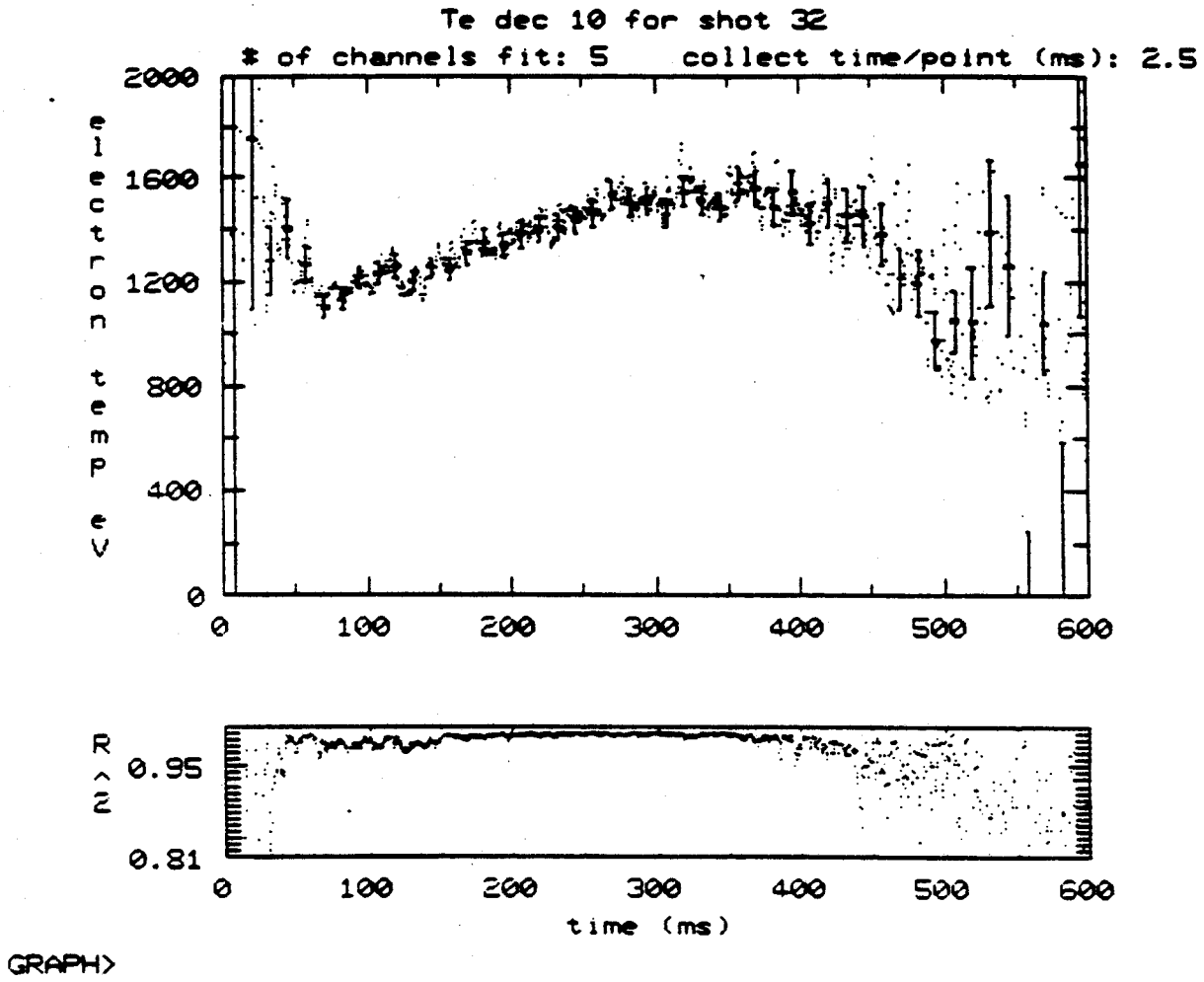

Figure 17
Upper: Electron Temperature vs Time
Lower: Goodness-of-Fit Parameter r^2 vs Time
Discharge #32 on December 10, 1983

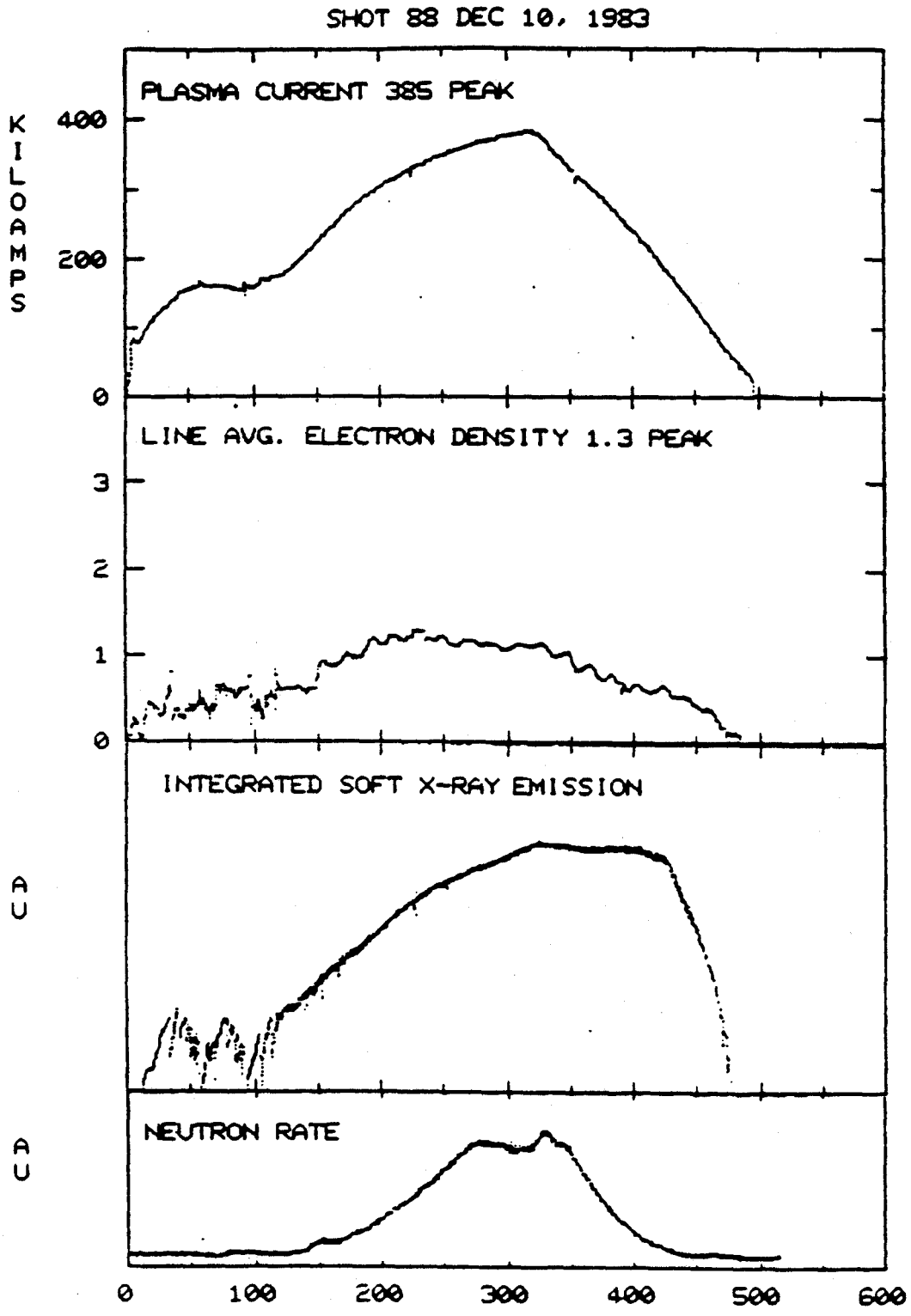

Figure 18
Plasma Current, Electron Density
Soft X-ray Flux and Neutron Rate
Discharge #88 on December 10, 1983

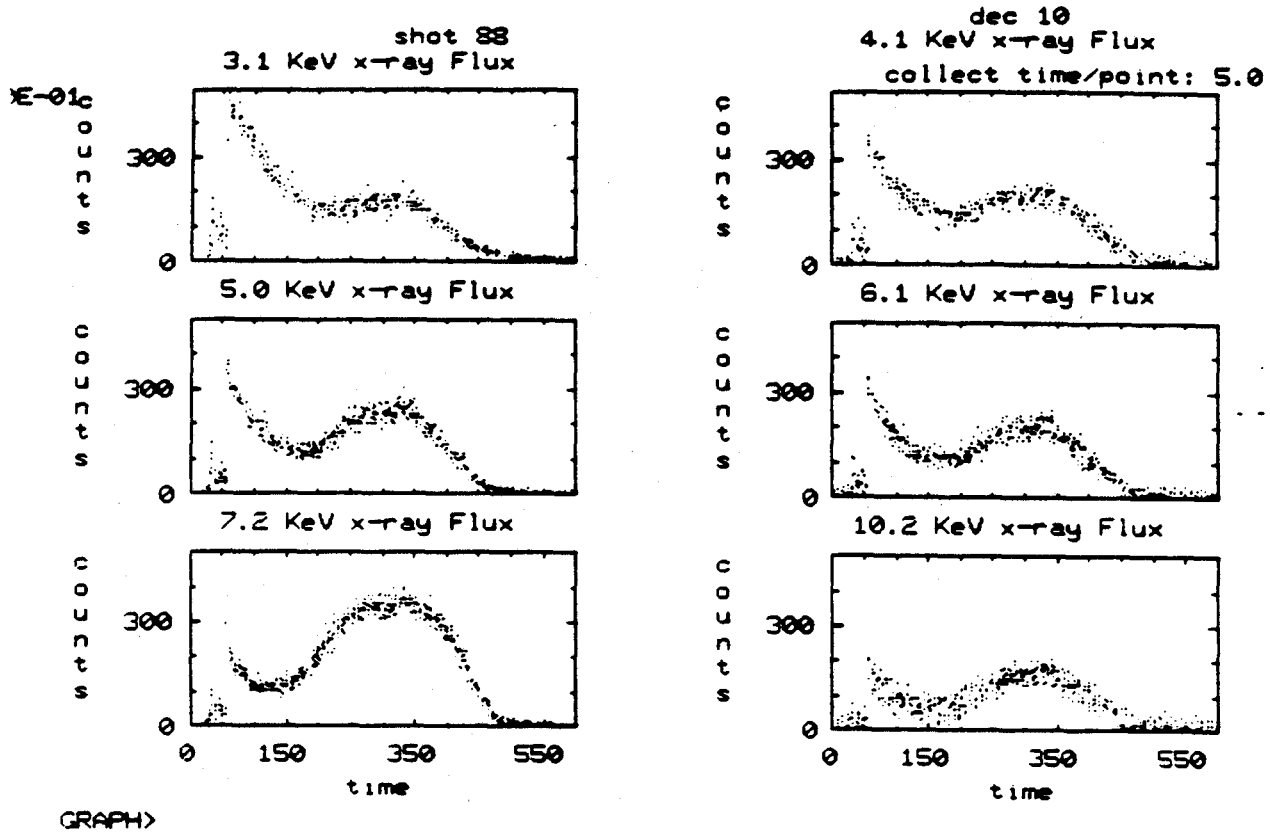

Figure 19
X-ray Flux in Each Monochrometer Channel vs Time
Discharge #88 on December 10, 1983

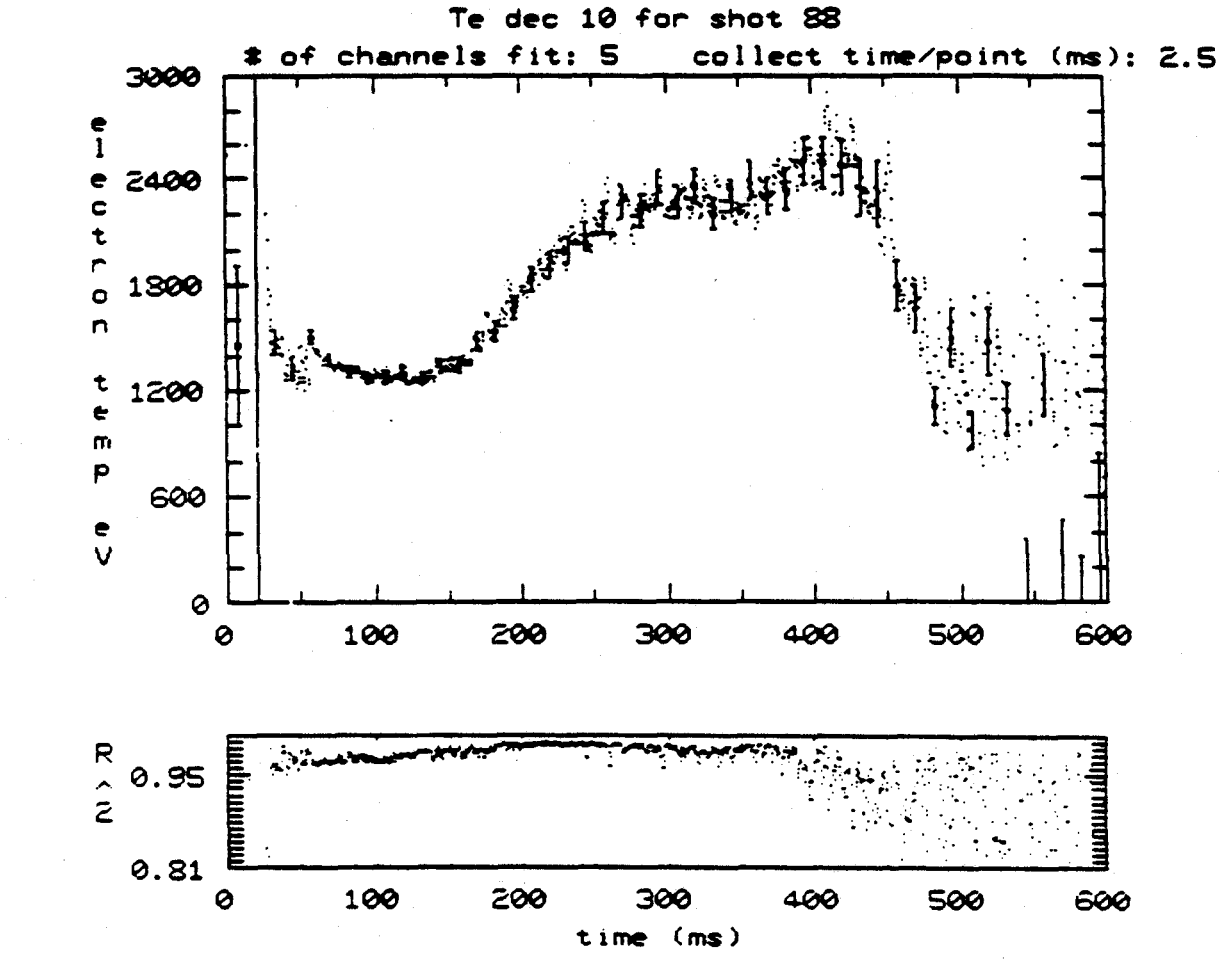

Figure 20
Upper: Electron Temperature vs Time
Lower: Goodness-of-Fit Parameter r^2 vs Time
Discharge #88 on December 10, 1983

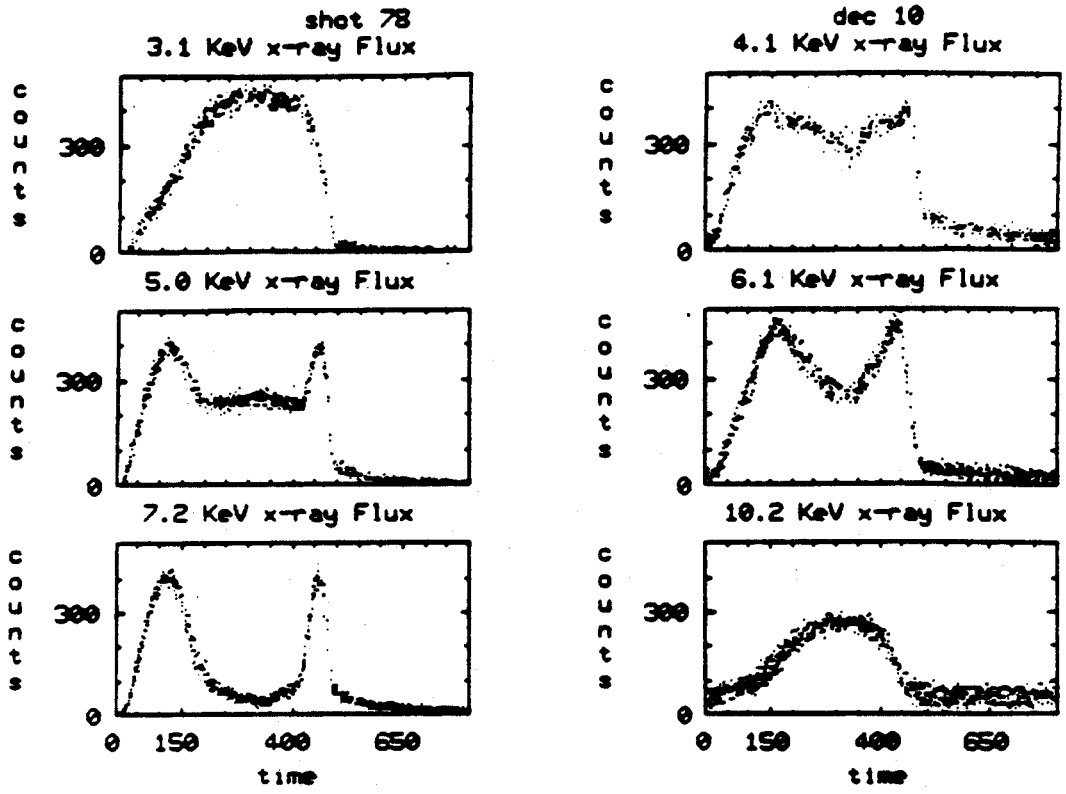

Figure 21
Partial Paralysis of Counting Mode Circuitry

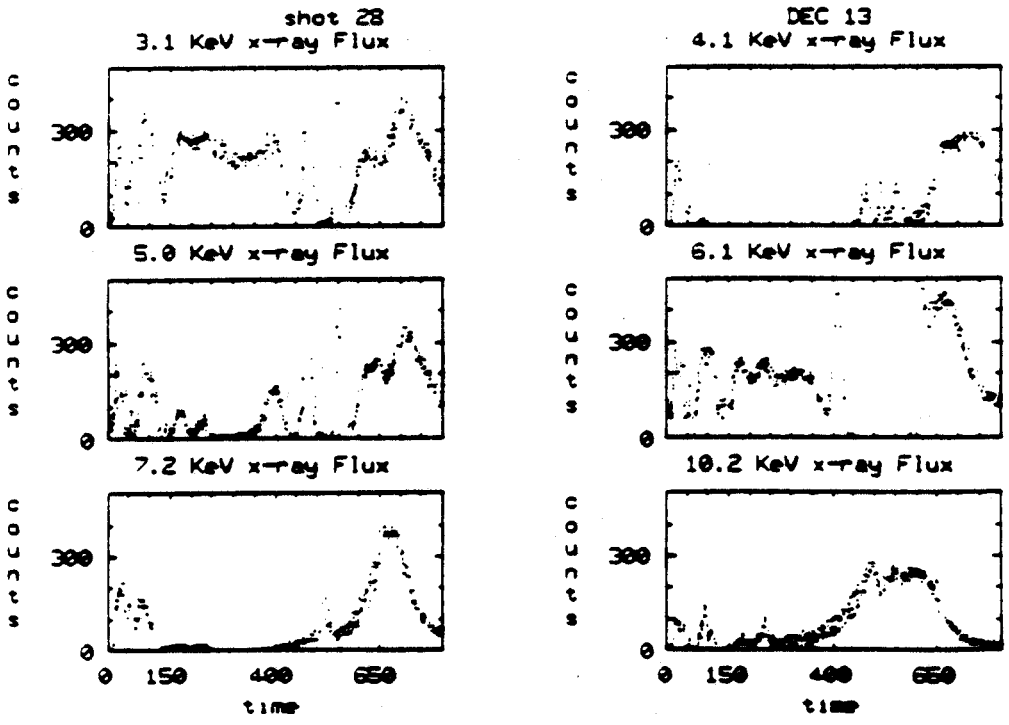

Figure 22
Complete Paralysis of Counting Mode Circuitry

Analog Mode Operation

Analog mode consists of amplifying the voltage produced across the anode resistor of each PMT and sampling the voltage periodically. The sampled voltages are digitized and the results stored in a memory. The memory has 3072 locations per channel, allowing 5 KHz sampling of the PMT signal. The method of calibration was the same as used for counting mode.

An interesting shot is shown in figure [23]. The density of the plasma was abruptly increased at 370 msec by firing a small pellet of frozen hydrogen into the plasma at 1 Km/sec. The pellet penetrated to near the center of the plasma where ablation released a burst of atoms that were quickly ionized. This large, sudden influx of cold particles cools the plasma momentarily. The sampled PMT signals are shown in figure [24]. The signals drop momentarily as the plasma cools, then rise sharply as the plasma reheats and the density increases. The reduced temperature trace is shown in figure [25]. There has been no correction for the 150 msec NaI fluorescence, and the error bars include only the error due to statistical fluctuations in the count rate. The peak count rate was near 7 MHz for this shot. The temperature drops when the pellet is fired, but quickly recovers. The reduced temperature near the pellet firing is shown in figure [26], and figure [27] shows the integrated soft x-ray flux for the same period. There are three sharp pulses in the temperature trace that do not show clearly on the soft x-ray trace. The next tempera-

ture excursion correlates well with a sawtooth visible on the total flux, and the next sawtooth is also visible, although not as well. This figure demonstrates the ability of the instrument to resolve electron temperature changes on the order of a millisecond in length and a hundred eV in size.

The primary drawback of analog mode operation is its limited dynamic range. The digitization is carried out to 12 bits resolution, giving a maximum dynamic range of 4096. The accuracy of the digitizer is closer to 10 bits. This limit on dynamic range means that no one setting of PMT bias will suffice to measure all discharges. On December 16, 1983, ALCATOR had a run in which traces of neon gas were introduced into the plasma as an aid in study of impurity confinement and transport. The resulting plasmas tended to be variable from shot to shot and disruptive during shots. PMT bias that was acceptable for one set of shots either saturated the tubes or gave very small signals a few shots later. The counting mode electronics, in contrast, worked well for all shots (except for pile-up). Even changes in the PMT bias voltage did not substantially affect counting mode performance.

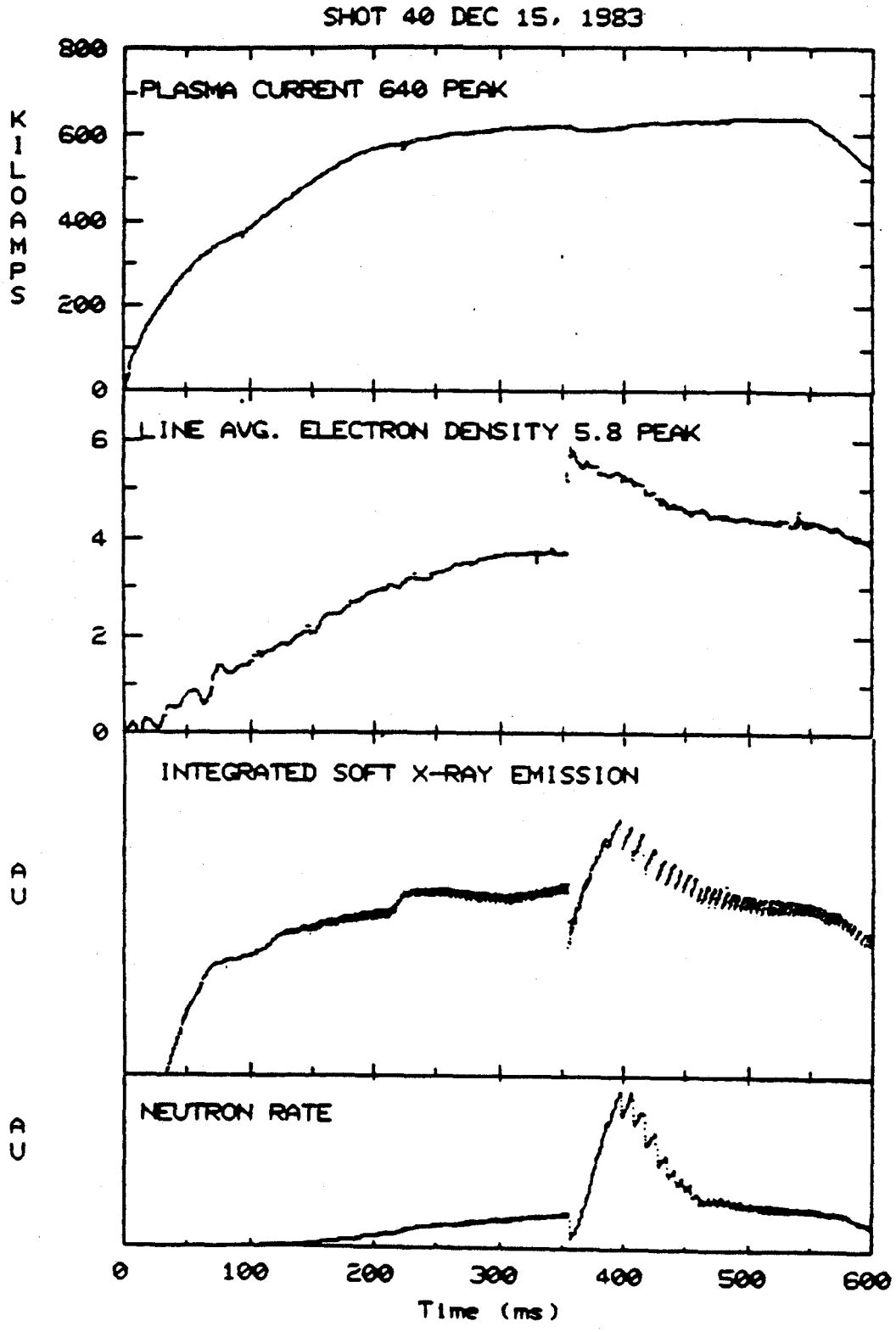

Figure 23
Plasma Current, Electron Density
Soft X-ray Flux and Neutron Rate
Discharge #40 on 15 December, 1983

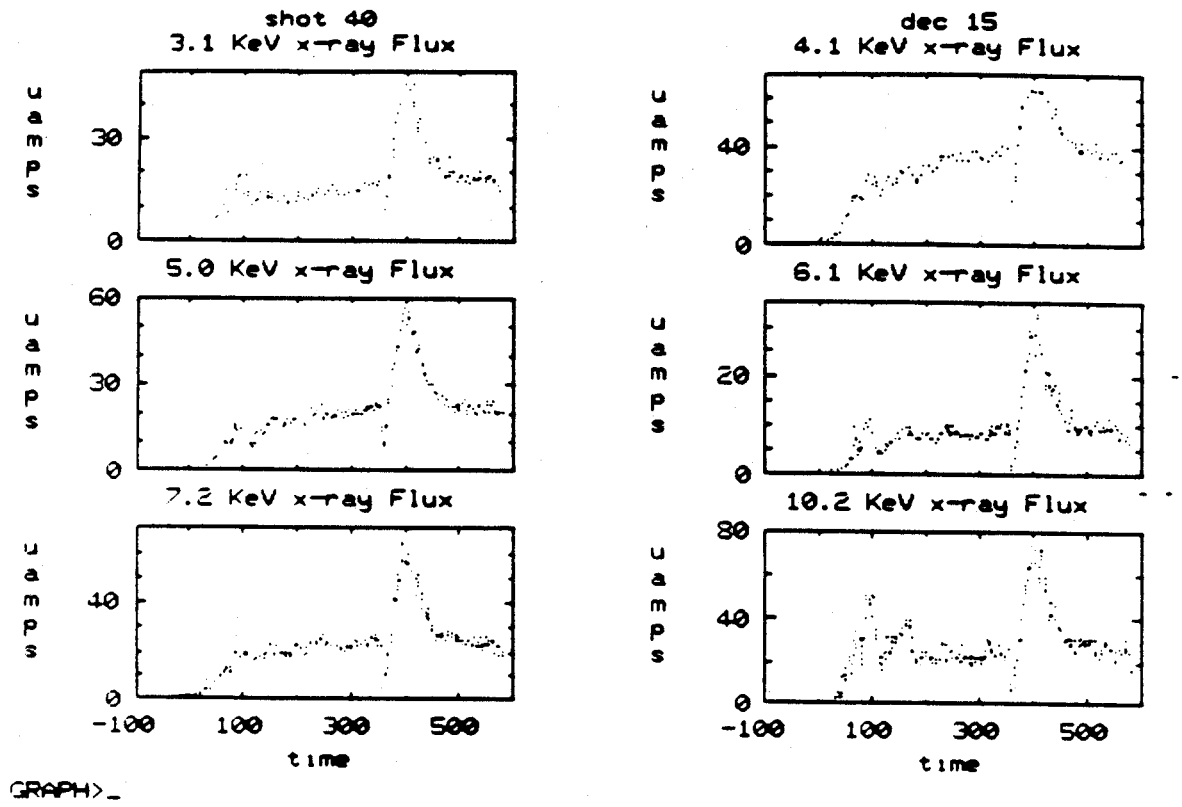

Figure 24
X-ray Flux in Each Monochrometer Channel vs Time
Discharge #40 on 15 December, 1983

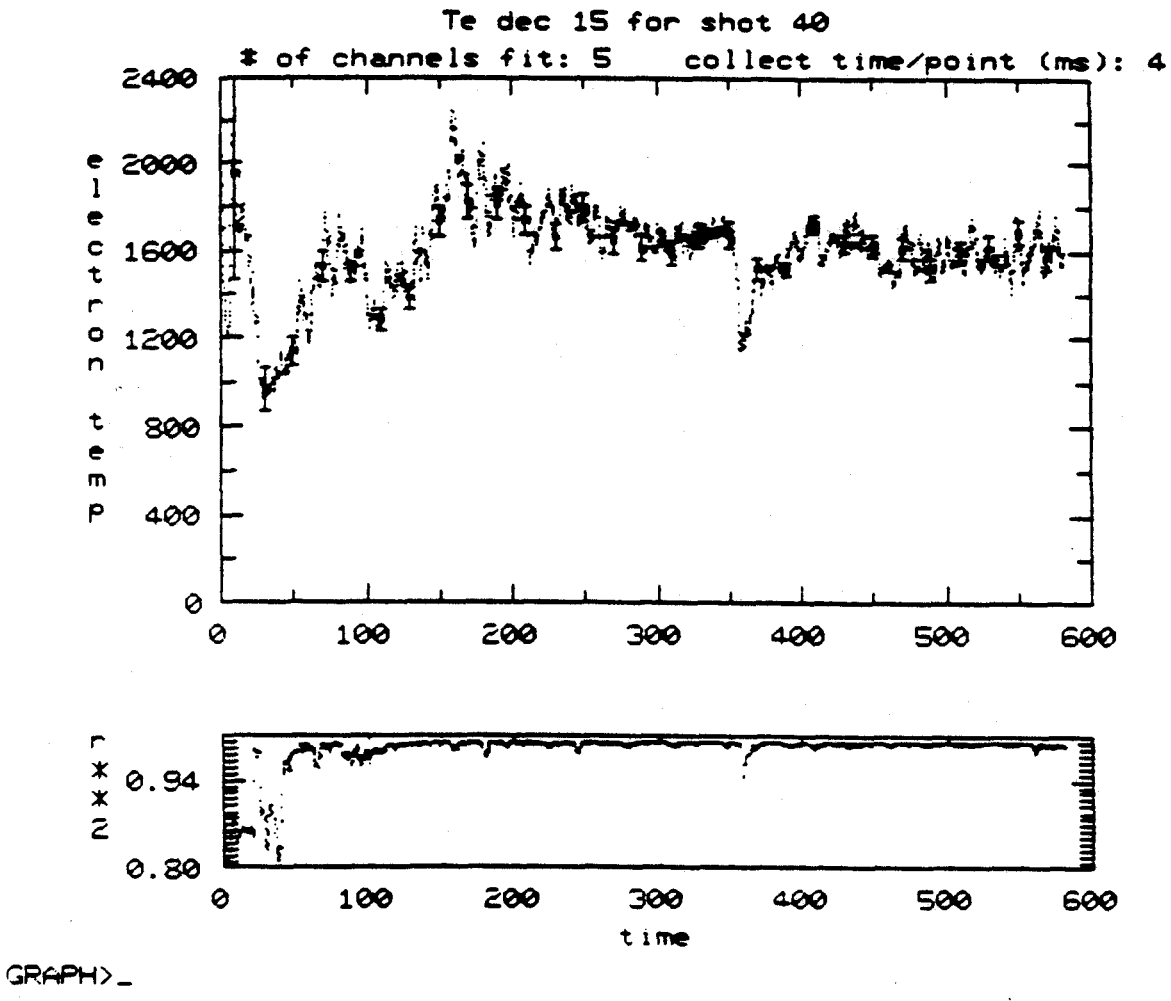

Figure 25
Upper: Electron Temperature vs Time
Lower: Goodness-of-Fit Parameter r^2 vs Time
Discharge #40 on 15 December, 1983

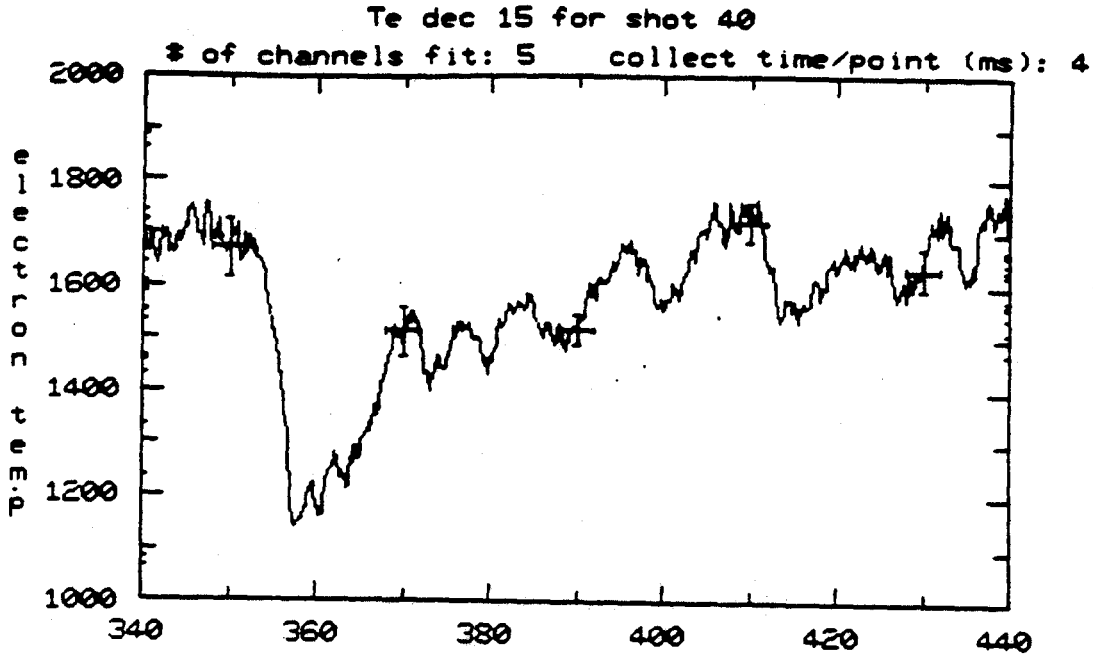

Figure 26
Electron Temperature Near Time of Pellet Injection

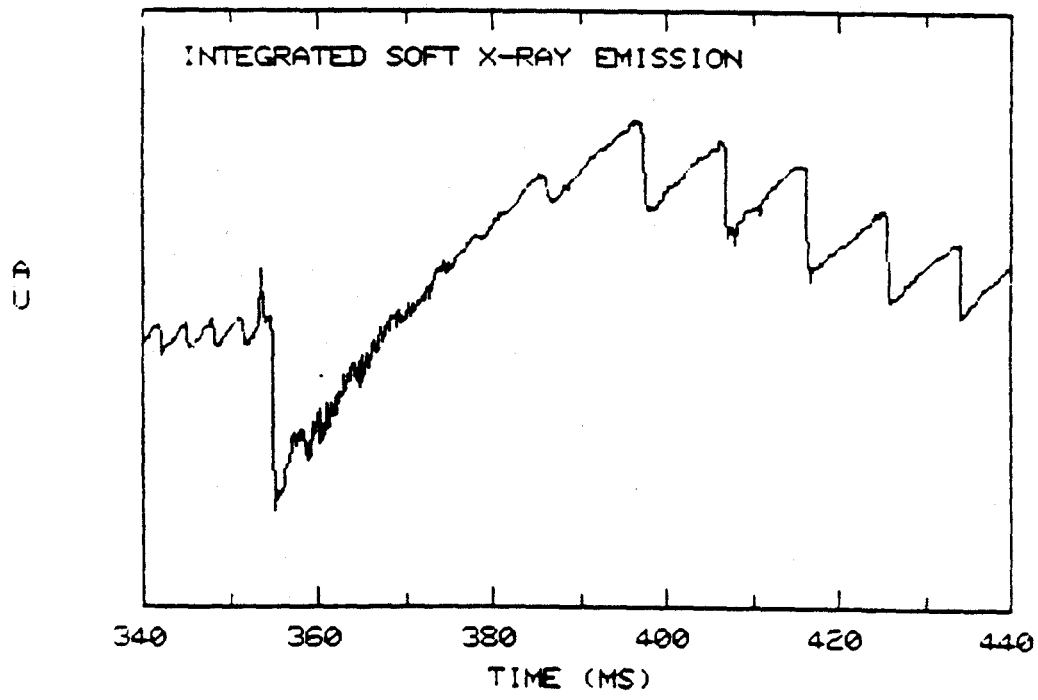

Figure 27
Plasma Soft X-ray and Neutron Emission Near
Time of Pellet Injection

FUTURE WORK

While the x-ray polychrometer approach to measuring the electron temperature has been demonstrated in principle, much work remains to develop the idea into a dependable, useful diagnostic. The first order of business is to fix the problems that arose during these experiments.

The problem of paralysis of the counting circuitry can be easily overcome with AC-coupled electronics. A properly designed circuit should accept counting rates up to 5 MHz. Delay-line pulse shaping, in which a portion of the signal is delayed and subtracted from the original signal, has the advantage that a large burst of light (as from a hard x-ray stopping in the scintillator) will give a single output pulse of the same width as any other. D.A. Landis at Los Alamos National Laboratory has implemented such a circuit for use as a pulse detector on the Si(Li) system of the Tokamak Fusion Test Reactor at Princeton Plasma Physics Laboratory [26].

The problem of limited dynamic range in the analog mode could be partially overcome with a logarithmic quantizer. Unfortunately, no such quantizers are commercially available in CAMAC hardware, so a custom circuit must be designed and built. The custodians of the CAMAC serial highway at ALCATOR are understandably reluctant to use non-commmercial hardware. Simply using a logarithmic amplifier in front of a linear quantizer will result in aliasing.

The contribution of the NaI(Tl) 150 msec fluorescence should be confirmed by observing the PMT signals after a plasma current disruption. If a disruption occurs immediately after pellet fueling, there will a very large impulse of x-rays into the polychrometer, and the signals will continue after the plasma current has returned to 0. The actual fluorescence contribution can then be measured. The PMT signals can be corrected for the effects of the fluoresence by convolving an appropriatly weighted 150 msec time-constant exponetial with the obseved signal, and subtracting the result of the convolution from the input signal. This method is only approximate because it uses the "contaminated" signal to estimate the true input signal, but should work well so long as the contribution of the fluorescence is small.

The problem of hard x-ray pickup in analog mode is not easily overcome. A more careful study of the problem is needed. If it is found that most of the pickup is due to x-rays of 200 KeV energy or less, then it should be possible to shield the system with tungsten or lead to reduce the problem. If the pickup is due to harder x-rays or to neutron scattering in the apparatus or $n\gamma$ reactions in the detector, then shielding will be difficult if not impossible.

ACKNOWLEDGEMENTS

The ALCATOR project is a team effort. Almost every member of the group has assisted me at one time or another, and that support is gratefully acknowledged.

Thanks to Professor Ronald Parker for his continuing financial and academic support.

John Rice provided much of the early stimulus for this work, as well as many informative discussions and the HgI spectra used to calibrate the instrument.

Elisabeth Kallne provided material, technical, and personal support for much of this work.

Stephen Wolfe, Dan Pappas, and Robert Granetz provided the density, neutron, and integrated soft X-ray traces, respectively. Jim Terry, David Gwinn, and Earl Marmar provided many stimulating discussions.

Ed Thibeault and his crew provided timely machine shop work when my measurements or foresight failed me.

Frank Silva held up the mirror now and then.

The superb technical staff of ALCATOR C deserves special thanks. They work from 5 am to 8 pm so that plasma is available from 9 to 5. They are always interested, helpful, and supportive. ALCATOR could not exist without them.

REFERENCES

[1] Tamm, I.E., Sakharov, A.D., Theory of Magnetic Thermonuclear Reactors (in two parts) AN SSR Fizika Plazmy i Problema Upravliaemykh Termoiadernikh Reaktsii, 1, 3, Moscow (1958)

[2] Sommerfeld, A., Maue, A., Ann. D. Phys. [5] 11 s.257 (1931)

[3] J. Greene Ap. J 130, 693, (1959)

[4] J. Karzas and R. Latter, Ap. J, Suppl 6, 167, (1961)

[5] Kissel, S.E., Thermal and Non-Thermal Submillimetre Emission From Alcator Tokamak, MIT Physics Sc.D Thesis, 1982

[6] Wolfe, S. Private Communication

[7] Menzel and Pekeris M.N.R.A.S. 96 77 (1938)

[8] Brussaard, P., Van de Hulst, H., Rev. Mod. Phys. 34 507 (1962)

[9] Von Goeller, S., MATT Report 1081 Princeton Plasma Physics Lab. (1975)

[10] Rice, J.E., MIT Physics Sc.D. Thesis, 1979.

[11] C. Bretin et al EVR-CEA-FC-948 1978

[12] Rice, J.E., Private Communication

[13] Tokamak Plasma Diagnostics De Michelis, ed., Nuclear Fusion 18 5 (1978)

[14] Watterson, Reich, private communication

[15] Roer, H., et al, Nuclear Fusion 22, no.8, p 1099 (1982)

[16] De Michelis, C., Papoular, R., Plasma Phys. 17 (1975) p. 1155

[17] Gandy, R.F., Yates, D., MIT Plasma Fusion Center PFC/RR 84-4 (1984)

[18] Compton, A.H., X-rays in Theory and Experiment D. Van Nostrand Company, New York, (1935)

[19] Bertin, E.P., Elements of X-Ray Spectrometric Analysis, Plenum Press, New York, 1978

[20] Kestenbaum, H.L., Appl. Spect. 27, 6, pp. 454-456 (1973)

[21] Birks, J.B., The Theory and Practice of Scintillation Counting, Pergammon Press Ltd., 1964

[22] Knoll, G.F. Radiation Detection and Measurement

[23] Petrasso, R., et al, "Plasma Impurity Reduction Following Pellet Injection," presented before the APSDPP, Los Angeles, CA, October 1983

[24] Terry, J.L., Private Communication

[25] Bevington, P.R., Data Reduction and Error Analysis for the Physical Sciences,McGraw-Hill 1969

[26] Goulding, F.S., Landis, D.A., Madden, N.W. IEEE Trans. Nucl. Science NS-30, no. 1, pp 301-310, Feb 1983

[27] Gilfrich, J.V., Brown, D.B., and Burkhalter, P.G., Appl. Spec. 29, 4, pp. 322-326 (1975)